

# Bone microstructure and the evolution of growth patterns in Permo-Triassic therocephalians (Amniota, Therapsida) of South Africa

Therocephalians were a speciose clade of nonmammalian therapsids whose ecological diversity and survivorship of the end-Permian mass extinction offer the potential to investigate the evolution of growth patterns across the clade and their underlying influences on post-extinction body size reductions, or 'Lilliput effects.' We present a phylogenetic survey of limb bone histology and growth patterns in therocephalians from the Middle Permian through Middle Triassic of the Karoo Basin, South Africa. Histologic sections were prepared from 80 limb bones representing 11 genera of therocephalians. Histologic indicators of skeletal growth, including cortical vascularity (%CV) and mean primary osteon diameters (POD), were evaluated in a phylogenetic framework and assessed for correlations with other biologically significant variables (e.g., size and robusticity). Changes in %CV and POD correlated strongly with evolutionary changes in body size (i.e., smaller-bodied descendants tended to have lower %CV than their larger-bodied ancestors across the tree). Bone wall thickness tended to be high in early therocephalians and lower in the gracile-limbed baurioids, but showed no general correlation with cross-sectional area or degree of vascularity (and, thus, growth). Clade-level patterns, however, deviated from previously studied within-lineage patterns. For example, *Moschorhinus*, one of few therapsid genera to have survived the extinction boundary, demonstrated higher %CV in the Triassic than in the Permian despite its smaller size in the extinction aftermath. Results support a synergistic model of size reductions for Triassic therocephalians, influenced both by within-lineage heterochronic shifts in survivor taxa (as reported in *Moschorhinus* and the dicynodont *Lystrosaurus*) and phylogenetically inferred survival of small-bodied taxa that had evolved short growth durations (e.g., baurioids). These findings mirror the multi-causal Lilliput patterns described in marine faunas, but contrast with skeletochronologic studies that suggest slow, prolonged shell secretion over several years in marine benthos. Applications of

phylogenetic comparative methods to new histologic data will continue to improve our understanding of the evolutionary dynamics of growth and body size shifts during mass extinctions and recoveries.

# **Bone microstructure and the evolution of growth patterns in Permo-Triassic therocephalians (Amniota, Therapsida) of South Africa**

Adam K. Huttenlocker\*

Department of Biology and Burke Museum of Natural History and Culture, University of  
Washington, Seattle, Washington 98195, U.S.A. Email: [ahuttenlocker@gmail.com](mailto:ahuttenlocker@gmail.com);

and

Jennifer Botha-Brink

Department of Karoo Palaeontology, National Museum and Department of Zoology and  
Entomology, University of the Free State, Bloemfontein 9300, South Africa; Centre of Excellence  
in Palaeosciences, University of Witwatersrand, Johannesburg 2050, South Africa. Email:  
[jbotha@nasmus.co.za](mailto:jbotha@nasmus.co.za).

\*Corresponding author; Current address: Department of Biology, University of Utah, and Natural  
History Museum of Utah, Salt Lake City, Utah, USA 84112-0840

40 pages, 1 appendix, 2 tables, 7 figures, and 1 supporting file w/ 10 supporting figures

**Abstract**—Therocephalians were a speciose clade of nonmammalian therapsids whose ecological diversity and survivorship of the end-Permian mass extinction offer the potential to investigate the evolution of growth patterns across the clade and their underlying influences on post-extinction body size reductions, or ‘Lilliput effects.’ We present a phylogenetic survey of limb bone histology and growth patterns in therocephalians from the Middle Permian through Middle Triassic of the Karoo Basin, South Africa. Histologic sections were prepared from 80 limb bones representing 11 genera of therocephalians. Histologic indicators of skeletal growth, including cortical vascularity (%CV) and mean primary osteon diameters (POD), were evaluated in a phylogenetic framework and assessed for correlations with other biologically significant variables (e.g., size and robusticity). Changes in %CV and POD correlated strongly with evolutionary changes in body size (i.e., smaller-bodied descendants tended to have lower %CV than their larger-bodied ancestors across the tree). Bone wall thickness tended to be high in early therocephalians and lower in the gracile-limbed baurioids, but showed no general correlation with cross-sectional area or degree of vascularity (and, thus, growth). Clade-level patterns, however, deviated from previously studied within-lineage patterns. For example, *Moschorhinus*, one of few therapsid genera to have survived the extinction boundary, demonstrated higher %CV in the Triassic than in the Permian despite its smaller size in the extinction aftermath. Results support a synergistic model of size reductions for Triassic therocephalians, influenced both by within-lineage heterochronic shifts in survivor taxa (as reported in *Moschorhinus* and the dicynodont *Lystrosaurus*) and phylogenetically inferred survival of small-bodied taxa that had evolved short growth durations (e.g., baurioids). These findings mirror the multi-causal Lilliput patterns described in marine faunas, but contrast with skeletochronologic studies that suggest slow, prolonged shell secretion over several years in marine benthos. Applications of phylogenetic comparative methods to new histologic data will continue to improve our understanding of the evolutionary dynamics of growth and body size shifts during mass extinctions and recoveries.

51

## 52 Introduction



53 Mass extinctions are frequently followed by short-term reductions in body sizes of  
54 survivor lineages, a pattern known as the ‘Lilliput effect’ (Urbanek, 1993; Harries, Kauffman &  
55 Hansen, 1996). However, in the absence of adequate phylogenetic and life history data, the  
56 mechanisms of size reductions can be unclear and may differ across environments, taxonomic  
57 groups, and extinction events (Twitchett, 2007; Harries and Knorr, 2009). Lilliput patterns have  
58 been documented widely in marine invertebrate groups following the end-Permian extinction  
59 (Payne, 2005; Twitchett, 2007; Luo et al., 2008; Mutter and Neuman, 2009; Metcalfe, Twitchett  
60 & Price-Lloyd, 2011; Song, Tong & Chen, 2011; Rego et al., 2012), and anecdotally in tetrapods  
61 of the Triassic *Lystrosaurus* Assemblage Zone in the Karoo Basin of South Africa (ca. 252.3 Ma),  
62 but growth dynamics underlying these patterns are not fully understood. Therocephalians  
63 represent an exemplary clade of nonmammalian therapsids that thrived from the Middle Permian  
64 to Middle Triassic, and survived the end-Permian extinction as important components of Triassic  
65 survivor and recovery faunas in the Karoo Basin (Botha and Smith, 2006). In addition to the  
66 dicynodont *Lystrosaurus*, at least three genera of therocephalians in two major groups have  
67 observed stratigraphic occurrences that span the extinction boundary in the Karoo: the baurioid  
68 *Tetracynodon*, and the akidnognathids *Promoschorhynchus* and *Moschorhinus* (Smith and Botha,  
69 2005; Botha and Smith, 2006; Huttenlocker, Sidor & Smith, 2011). Other Triassic taxa (e.g.,  
70 *Olivierosuchus*, *Regisaurus*) have long ghost lineages extending into the Permian, indicating that  
71 they too survived the extinction but lack a Permian record within the depositional basin  
72 (Huttenlocker, 2009; Huttenlocker, Sidor & Smith, 2011). Although therocephalians are generally  
73 exceeded in abundance by dicynodont therapsids in the Karoo Basin, their diversity, extensive  
74 stratigraphic range, and success during the end-Permian extinction make them an ideal group to

study evolutionary patterns during the Permian-Triassic transition.

Previous morphological studies of therocephalians have emphasized their functional anatomy, including jaw mechanics and locomotory specializations (e.g., Kemp, 1972, 1978, 1986; Fourie and Rubidge, 2007, 2009). Recent collaborative work on therocephalians has emphasized integration of their fine structure and internal anatomy to resolve paleobiological questions, including tooth replacement patterns, braincase structure, and growth and histomorphologic structure (Abdala, Rubidge & van den Heever, 2008; Sigurdson et al., 2012; Huttenlocker and Botha-Brink, 2013). Detailed investigations of histomorphology are particularly useful, permitting assessments of growth patterns and variation within or among closely related therapsid species (e.g., Botha and Angielczyk, 2007; Huttenlocker and Botha-Brink, 2013). Moreover, as growth patterns are associated with organismal fitness, recent investigations into bone microstructure have inquired into whether certain growth strategies conferred success on some groups during the end-Permian mass extinction (e.g., rapid growth in the dicynodont *Lystrosaurus* and its relatives; Botha-Brink and Angielczyk, 2010).

### **Bone Microstructure in Therapsids**

Bone histology has offered insights into the lifestyles and growth patterns of many of the major subclades of nonmammalian therapsids. Recent examples include investigations of feeding and locomotion, habitat use, and especially growth dynamics (e.g., Ray, Chinsamy & Bandyopadhyay, 2005; Jasinowski, Rayfield & Chinsamy, 2010; Chinsamy-Turan, 2012). Earlier surveys of bone histology emphasized differences between basal (pelycosaurian-grade) synapsid and therapsid tissue composition, matrix organization, and degree of vasculature of the limb bones (Enlow and Brown, 1957; Enlow, 1969; Ricqlès, 1969, 1974a, 1974b, 1976). Particularly, fibrolamellar tissue complexes (vascularized bone tissues that incorporate primary osteons within a woven-fibered matrix) were found to be near ubiquitous among limb elements of sampled therapsids, suggesting that this tissue complex appeared early during therapsid evolution prior to

100 the origination of mammals bearing this tissue-type (Ricqlès, 1969, 1974a, b; Ray, Botha &  
 101 Chinsamy, 2004; Chinsamy and Hurum, 2006; Ray, Bandyopadhyay & Bhawal, 2009). Indeed,  
 102 fibrolamellar bone has been reported  basal therapsids (e.g., *Biarmosuchus*: Ricqlès, 1974b), as  
 103 well as in ~~some~~ **immature pelycosaurian**-grade synapsids (~~e.g.,~~ *Sphenacodon* and *Dimetrodon*  
 104 ~~juveniles~~) and in fast-growing portions of the skeleton (e.g., the elongated neural spines of  
 105 *Dimetrodon* and crossbars on the neural spines of *Edaphosaurus*) (Huttenlocker, Rega & Sumida,  
 106 2010; Huttenlocker, Mazierski & Reisz, 2011; Huttenlocker and Rega, 2012; Shelton et al.,  
 107 2013). However, there is great histovariability in the organization of fibrolamellar bone even  
 108 within major subclades of therapsids. Fibrolamellar bone may be formed by varying degrees of  
 109 woven- and parallel-fibered interstitial matrix and incorporates a variety of vascular motifs, and  
 110 may be zonal (punctuated by cyclic growth marks) or azonal. Ray, Botha & Chinsamy (2004)  
 111 reported the presence of zonal fibrolamellar bone in many Permian  Middle Triassic taxa, but  
 112 suggested that sustained (non-cyclic) growth patterns **might have arisen** occasionally in a number  
 113 of phylogenetically disparate taxa that do not encompass the immediate ancestors of mammals  
 114 (gorgonopsian *Aelurognathus*; eucynodont *Cynognathus*; and some bidentalians dicynodonts). The  
 115 abundance of dicynodont fossils in Permian and Triassic rocks and recent advances in their  
 116 systematic relationships have permitted more detailed comparisons of growth patterns in this  
 117 diverse subclade (Chinsamy and Rubidge, 1993; Botha, 2003; Ray and Chinsamy, 2004; Ray,  
 118 Chinsamy & Bandyopadhyay, 2005; Botha and Angielczyk, 2007; Ray, Bandyopadhyay &  
 119 Bhawal, 2009; Botha-Brink and Angielczyk, 2010; Green, Schweitzer & Lamm, 2010;  
 120 Nasterlack, Canoville & Chinsamy-Turan, 2012; Ray, Botha-Brink & Chinsamy-Turan, 2012).  
 121 Phylogenetic comparative surveys have revealed patterns of increasing tissue vascularity during  
 122 the evolutionary history of bidentalians dicynodonts (especially in Triassic forms like  
 123 *Lystrosaurus*), and determinate growth patterns with peripheral rest lines and systematic cortical  
 124 remodeling in large kannemeyeriiforms (Botha-Brink and Angielczyk, 2010; Green, Schweitzer

125 & Lamm, 2010; Ray, Botha-Brink & Chinsamy-Turan, 2012).

126       The diversity of growth patterns in other nonmammalian therapsid groups, as well as their  
127 phylogenetic and temporal distributions, is incompletely known. A body of literature on  
128 nonmammalian cynodont histology has accrued in recent years (e.g., Ricqlès, 1969; Botha and  
129 Chinsamy, 2000, 2004, 2005; Ray, Botha & Chinsamy, 2004; Chinsamy and Abdala, 2008;  
130 Botha-Brink, Abdala & Chinsamy-Turan, 2012), but sampling has been more limited in other  
131 theriodonts, such as the gorgonopsians and therocephalians (Ray, Botha & Chinsamy, 2004;  
132 Chinsamy-Turan and Ray, 2012). Ricqlès (1969) suggested differential rates of growth between a  
133 basal therocephalian from the Middle Permian of South Africa and the Late Permian whaitsiid  
134 ‘*Notosollasia*’ (= *Theriognathus*). Given the comparatively more vascularized cortical bone in the  
135 radius of the whaitsiid (1969: plate IV), Ricqlès suggested that therocephalians might have  
136 exhibited accelerated growth rates later in their evolutionary history, paralleling the  
137 aforementioned temporal pattern of increasing growth rates in some dicynodonts. More recently,  
138 Ray, Botha & Chinsamy (2004) and Chinsamy-Turan and Ray (2012) analyzed additional  
139 material from an indeterminate scylacosaurid (erroneously identified as ‘*Pristerognathus*’) and  
140 argued for similar ‘flexible’ growth patterns in gorgonopsians, basal therocephalians, and most  
141 early cynodonts. The authors suggested that more rigorous taxonomic sampling would better  
142 substantiate parallel trends toward a loss in developmental plasticity and acceleration of growth  
143 rates as in dicynodonts. Inadequate sampling of eutheriocephalians before and after the end-  
144 Permian mass extinction limits our understanding of evolutionary patterns in therapsid  
145 histomorphology and skeletal growth during this important geologic transition.

## 146 **Present Study**

147       Although eutheriocephalians have not been sampled histologically for such comparisons,  
148 recent revisions to Permo-Triassic boundary-crossing taxa have necessitated cursory descriptions  
149 of eutheriocephalian histology for its ontogenetic and paleobiological implications (e.g.,



150 *Tetracynodon*: Sigurdson et al., 2012; *Moschorhinus*: Huttenlocker and Botha-Brink, 2013).

151 During the course of this work, we developed a database of histological data and images with the

152 goal of addressing features of life history evolution in Permian and Triassic eutheriodonts

153 (therocephalians and cynodonts), particularly in the context of the end-Permian extinction. Here,

154 we present a reappraisal of limb bone microstructure in Permian and Triassic therocephalians

155 based on new histologic sampling, and offer a hypothesis of the evolution of their growth

156 patterns. We suggest that therocephalians provide a robust study system for investigating the

157 evolution of growth strategies during the Permian-Triassic transition, and a useful point of

158 comparison and contrast to other groups that lived during this time (e.g., dicynodonts,

159 cynodonts).

160

## 161 **Materials and Methods**

### 162 **Specimen Selection and Histological Processing**

163 Specimens were selected based on completeness and availability for histological

164 processing, but a broad sample of the major representatives of South African therocephalians was

165 desired in order to recognize long-term patterns (if present) or clade specific histomorphology.

166 Specimens that were semi-articulated and included diagnostic cranial material were preferred for

167 accuracy of taxonomic identifications. Some specimens were not diagnosable to genus, but were

168 resolved to their respective higher taxon as in the case of five indeterminate scylacosaurids

169 described here. Scylacosaurids are generally difficult to identify unless a complete and accurate

170 antecanine tooth count can be made, and some authors have suggested that the diversity of

171 scylacosaurids is over-split because variations in tooth count may be ontogenetically variable

172 (e.g., Abdala, Rubidge & van den Heever, 2008). The sample therefore included 80 limb elements

173 from 33 individuals in 11 genera: *Lycosuchus*, *Glanosuchus*, *Moschorhinus*, *Olivierosuchus*,

174 *Hofmeyria*, *Mirotenthes*, *Theriognathus*, *Ictidosuchoides*, *Tetracynodon*, *Scaloposaurus*, and  
175 *Microgomphodon* (Fig. 1), plus additional scylacosaurid material ~~not diagnosed to genus~~. Thin-  
176 sections were prepared using standard histological techniques modified from Chinsamy and  
177 Raath (1992) and Wilson (1994). Limb bone midshafts were sampled cross-sectionally and  
178 imaged using Nikon Eclipse 50i and LV100 POL petrographic microscopes with a digital image  
179 capture system. Histomorphometric variables (discussed below) were measured using NIS-  
180 Elements and NIH ImageJ v. 1.42q software (Rasband, 1997-2012). *Moschorhinus*  
181 histomorphology was excluded from present description as it has been discussed elsewhere  
182 (Huttenlocker and Botha-Brink, 2013), but data from *Moschorhinus* were included in the  
183 quantitative analyses (Table 1).

#### 184 **Bone Tissue Typology: Definitions and Selection of Growth Proxies**



185 Bone tissue texture exhibited marked variation in therocephalians and other therapsids,  
186 varying from highly organized and lamellar to disorganized and woven. Only a few recent studies  
187 have integrated qualitative and quantitative assessments of tissue texture and vascular proxies of  
188 growth in Permo-Triassic therapsids (Botha and Chinsamy 2000, 2004, 2005; Ray and Chinsamy  
189 2004; Ray et al., 2004, 2005, 2010; Botha-Brink and Angielczyk 2010; Huttenlocker and Botha-  
190 Brink, 2013). Generally, cellular bone forms as osteoblasts become incorporated into the  
191 extracellular (or interstitial) matrix (ECM) forming quiescent osteocytes. The overall bone  
192 apposition rate affects the texture of the mineralized ECM, with collagen fibers and crystallites  
193 bearing a more lamellar organization under slower growth and a nonlamellar (woven-fibered)  
194 texture under faster growth. Parallel-fibered bone, an intermediate tissue-type, can be identified  
195 by its ‘streaky’ appearance under polarized light, with the predominant fiber orientation being  
196 parallel to the surface of the bone and forming a woven-basket texture in most cases. In cases in  
197 which birefringent properties have been disrupted by diagenetic processes, it is possible to  
198 approximate the relative organization of mineralized fibers with reference to the organization of

199 the lacunocanalicular network within the ECM (Stein and Prondvai, 2013). In contrast to parallel-  
 200 fibered bone, woven-fibered bone includes large, globular osteocyte lacunae that are usually  
 201 densely packed within the mineralized ECM. Nonlamellar tissues (parallel- and woven-fibered)  
 202 may also frequently incorporate large vascular canals that later become infilled with one or two  
 203 concentric lamellae forming primary osteons (diagnosed by their ‘Maltese cross’ pattern of  
 204 birefringence under polarized light). These tunnels form passageways for blood vessels and  
 205 nerves while also contributing to the structural integrity of the bone by providing added bone  
 206 mass and helping to blunt microcracks (Currey, 2002). The result is a fibrolamellar bone complex  
 207 (herein ‘FLB’), in which a disorganized, fibrous or nonlamellar interstitial matrix incorporates an  
 208 anastomosing network of centripetally lamellated primary osteons. Currey (1987, 2002) defined  
 209 FLB broadly as a tissue complex formed by parallel- (or woven-) fibered bone with primary  
 210 osteons (2002: p.18). By contrast, Ricqlès (1974a) originally restricted the term ‘fibrolamellar’ to  
 211 tissues formed largely by woven-fibered bone with primary osteons, excluding parallel-fibered  
 212 bone from this category. Herein, we follow the traditional usage of Ricqlès, but temper this strict  
 213 definition by noting that parallel- and woven-fibered bone form a continuum that is often ill-  
 214 defined (and may be present simultaneously in many therapsid bony tissues, even within the same  
 215 section). Bone cortices formed primarily by lamellar tissue, which forms at relatively slower  
 216 apposition rates (~1  $\mu\text{m}/\text{day}$  or less), do not typically incorporate primary osteons, instead  
 217 bearing simple vascular canals or being avascular. In lamellar bone, the lacunocanalicular  
 218 network is ordered, the osteocyte lacunae being small and more lacunar in appearance with the  
 219 long axis oriented parallel to the surface of the bone. Both tissue complexes can be zonal  
 220 (periodically interrupted by growth marks) or azonal. Growth marks in zonal bone may be  
 221 present in the form of lines of arrested growth or ‘LAGs’ (denoted by an opaque cement line,  
 222 traceable around the entire cortex, and indicative of a temporary cessation of growth) or annuli  
 223 (thin bands of dense, annular tissue, usually parallel-fibered or lamellar, deposited during periods

224 of slowed growth).

225 For quantitative histomorphometric analysis, two vascular proxies of skeletal growth were  
 226 selected: cortical vascularity and mean primary osteon diameter. These proxies were selected in  
 227 order to evaluate the extent to which histological correlatives of growth varied across phylogeny,  
 228 and whether their ~~evolution was~~ tied to body size or other biological factors. Vascular proxies  
 229 have offered useful indicators of skeletal growth in extant and extinct tetrapods (Castanet et al.,  
 230 2000; Margerie et al., 2002, 2004; Buffrénil, Houssaye & Böhme, 2007; Cubo et al., 2012), and  
 231 their utility here allows comparisons with other histological studies of therapsids in which similar  
 232 measures were used (e.g., Botha-Brink and Angielczyk 2010; Huttenlocker and Botha-Brink,  
 233 2013). Notably, ontogenetic variation in growth may introduce a lesser degree of cortical  
 234 vascularity in adult bones that exhibited decreasing apposition rates prior to death and burial, or  
 235 may introduce variation in a single cross-section. Nonmammalian therapsids, however, are well  
 236 suited to relative growth rate estimation based on tissue texture and vascularity, due to their  
 237 generally thick bone walls (preserving the early record of primary growth) and limited secondary  
 238 remodeling (Botha-Brink and Angielczyk, 2010). Measurement of cortical vascularity (%*CV*, the  
 239 relative area of the cortex that is occupied by porous, vascular spaces) follows Lee et al. (2013).  
 240 Measurements were restricted to the inner two-thirds to three-quarters of the cortex where the  
 241 bone formed at high, sustained growth rates (Cubo et al., 2012), and were averaged from ten  
 242 quadrants sampled circularly around each midshaft cross-section. The subsampled quadrants  
 243 excluded areas of secondary reconstruction and outer regions of simple canals. We also estimated  
 244 mean primary osteon diameter (*POD*) by measuring in microns the transverse (or minimum)  
 245 widths of 15 primary osteons visible in the subsampled regions and averaging them across all  
 246 regions within a given midshaft cross-section.

247 To examine potential effects of size and robusticity on measured histomorphometric  
 248 variables, we also estimated two proxies of overall bone robusticity: *K* and relative bone wall

thickness (*RBT*). These variables play a frequent role in histological studies of fossil tetrapod bone, as bone robusticity may correspond to habitat preferences or mechanical loading (Wall, 1983; Currey and Alexander, 1985; Currey, 2002; Laurin, Girondot & Loth, 2004; Germain and Laurin, 2005; Kriloff et al., 2008). However, their relationships to size, growth, and vascularity have been underexplored in a comparative framework. Whereas  $K$  represents the proportional diameter of the medullary region relative to the total diameter of the cross-section (Currey and Alexander, 1985), *RBT* represents a percentage of the average cross-sectional thickness of the bone wall relative to the total diameter of the cross-section (Chinsamy, 1993). These measurements, as well as cross-sectional area at midshaft, were attained using NIH ImageJ, and were tested for correlations with vascular growth proxies using Pearson's product-moment correlation tests. Histomorphometric data are recorded in Table 1.

## Correlation Tests

**Pearson's product-moment correlation tests**—We performed a series of correlation tests in order to evaluate the extent to which variations in vascular growth proxies were dependent upon size and robusticity, which bear a strong influence on many aspects of organismal biology (Peters, 1983; Calder, 1984; Stearns, 1992). For instance, small-bodied therocephalians might have achieved their increasingly diminutive sizes by having a slower growing, less vascularized skeleton compared to their larger-bodied predecessors. In this scenario, one would expect a correlation between smaller size and slower growth, and between larger size and faster growth across subclades. ~~In extant vertebrates, small-bodied species generally exhibit slower growth rates than larger-bodied groups (Case, 1978), a general feature that has also been identified from histologic data in~~ fossil non-avian dinosaurs (Erickson et al., 2004; Lee, 2007). On the other hand, smaller sizes may have been achieved by shortening the duration of the growth period, in which case no generalized correlations between size and vascular proxies of skeletal growth are necessary. To address these hypotheses,

histomorphometric data (%*CV*, *POD*, *RBT*) and midshaft cross-sectional area were recorded for each sectioned limb bone. The data were organized into propodial, epipodial, and pooled subsets to control for the effects of increased variance from pooling limb bones of different types (although the effects appeared to be minimal as all tests ultimately yielded similar results). For each data partition, Pearson's product-moment correlation tests were performed between histomorphometric variables (%*CV*, *POD*, *RBT*) and the natural log of midshaft cross-sectional area. Vascular growth proxies were also tested for correlations with bone robusticity independent of size, and with each other to assess whether %*CV* and *POD* provided comparable estimates of vascularization.

**Phylogeny-independent contrasts**—Independent contrast methods were carried out to control for the effects of phylogenetic non-independence of putative correlations (Felsenstein, 1985; Garland, Bennett & Rezende, 2005). For example, one might find low tissue vascularity in Triassic baurioids due to their generally small sizes, or due to their close relatedness (and, by extension, their inherited phenotypic similarities). We carried out additional correlation tests on an augmented data set using the PDAP:PDTree module (Midford et al., 2011) in Mesquite version 2.0 (Maddison and Maddison, 2007). This required a tree and branch lengths (adapted from Huttenlocker, 2013 and [in press](#)) pruned to the 11 histologically sampled taxa. First, tip data for each of the 11 taxa were recorded in a NEXUS file, including average %*CV*, *POD*, *RBT* and the natural log of midshaft area of the propodials and epipodials separately (limb bones were not pooled for independent contrasts). Second, ancestral character states (estimated using squared-change parsimony) were checked for the assumption of Brownian motion evolution that governs independent contrasts (Felsenstein, 1985; Díaz-Uriarte and Garland, 1996). This was performed by running assumption-testing operations in PDAP that evaluate the relationship between the absolute values of independent contrasts and their corresponding standard deviations. Non-significant relationships were determined for each of the data partitions, indicating that a

Brownian motion model adequately fit the tip data. Finally, the same sets of regressions were performed on independent contrasts as in the untransformed data (size, robusticity, and vascular growth proxies).

## Results

### Results1: Qualitative Histomorphology

Due to space limitations, the present description is accompanied by a more detailed account in the Supporting Data file. In general, limb bone cortices in studied therocephalians were thick and formed primarily by FLB with varying degrees of vascularization, depending on size and phylogenetic position. For example, large basal therocephalians from the Middle Permian exhibited subplexiform FLB in the propodial elements with a comparatively high degree of vascularization ( $\%CV \sim 13\text{--}16\%$ ;  $POD \sim 75\text{--}168 \mu\text{m}$ ). By contrast, some smaller-bodied taxa in both the Permian and Triassic tended to incorporate more parallel-fibered bone or showed evidence of increased parallel-fibered and lamellar bone deposition with less vasculature toward the outer cortex, indicative of growth attenuation and attainment of somatic maturity (Margerie, Cubo & Castanet, 2002). This pattern is marked in *Mirotenthes*, which preserves an external fundamental system ('EFS') in some elements (an outer collar of avascular, generally acellular, lamellar bone indicative of virtual cessation of circumferential growth in adult individuals; Cormack, 1987; Huttenlocker, Woodward & Hall, 2013). Systematic cortical remodeling by Haversian bone formation was rare and only a few sparse secondary osteons were identified in some Permian scylacosaurian taxa [e.g., an indeterminate scylacosaurid and *Moschorhinus*, contrary to reports of extensive skeletal remodeling by Chinsamy-Turan and Ray (2012: p. 203)]. As in dicynodonts and other therapsids in which histology is well known, most basal therocephalians and euterocephalians exhibited remarkably thick bone walls ( $\sim 20\text{--}35\%$  *RBT* in



forelimb elements of lycosuchids, scylacosaurids, and akidnognathids; ~40% in forelimbs of hofmeyriids). This condition, however, was lost in baurioids, which were instead characterized by a much thinner cortical bone wall (< 25% in the forelimb and propodials) and more slender limb bones.

Permian basal therocephalians and euterocephalians (Fig. 2A–C, F, G; Fig. 3A, B) generally showed multiple growth zones as well, demarcated by cyclic growth marks indicative of periodic pauses in growth as in other Permian therapsids (Ray et al., 2004, 2012; Botha-Brink and Angielczyk, 2010; Botha-Brink et al., 2012). By comparison, Triassic therocephalians (Fig. 2D, E; Fig. 3C–F) showed a variety of vascular motifs and tissue-types (e.g., richly vascularized and disorganized bone tissues in akidnognathids; less vascularized parallel-fibered bone tissue in baurioids), but growth marks were less frequently recorded in all Triassic species. Small Triassic baurioids in particular showed thinner bone walls with few growth marks, less vascularized limb bone cortices, and smaller, more sparsely distributed primary osteons on average.

## Results 2: Quantitative Histometrics

**Pearson's correlation and phylogeny-independent contrasts**—Results of raw and phylogeny-corrected correlation tests are presented in Table 2. Correlation tests on raw data found that vascular growth proxies were strongly positively correlated with size [i.e., the natural log of midshaft cross-sectional area, underscoring greater overall tissue vascularity in large bones from larger taxa (e.g., *Lycosuchus*, scylacosaurids, *Moschorhinus*)] (Fig. 4; Table 2). Both %CV and *POD* also exhibited a strong positive correlation with each other, indicating that %CV and *POD* represent equivalent proxies for understanding relationships between bone tissue vascularization and growth across the therocephalian clade. Whereas the selected vascular growth proxies shared a consistent positive relationship with size for all data partitions, putative associations between robusticity and size were less clear. Correlation tests on raw size data and



*RBT* were non-significant. Likewise, correlation tests on raw vascular growth proxies and *RBT* either yielded non-significant *p*-values or, in the case of the propodial-only data partition, had low correlation coefficients with only a weakly positive association. This result is likely due to the fact that even some small-bodied taxa exhibited unexpectedly thick bone walls, as in the case of the hofmeyriids *Hofmeyria* and *Mirotenthes*. Bone wall thickness correlates poorly with size and growth proxies, suggesting that size and rate of growth may have had limited influence over bone robusticity as compared to other aspects of organismal biology such as mechanical regime (e.g., locomotor behavior, stance or gait; Currey & Alexander, 1985) and ecology or habitat preference (e.g., burrowing, semi-aquatic/aquatic; Wall, 1983; Laurin, Girondot & Loth, 2004; Germain and Laurin, 2005).

Results of phylogeny-corrected correlations further indicated a strong relationship between size and some histometrics (but not with limb bone robusticity) (Table 2). Evolutionary decreases in cross-sectional area of limb bones were generally associated with decreases in average %*CV* and *POD*. Eutherocephalians and particularly baurioids demonstrated a noteworthy pattern in which reconstructed ancestor-descendant size reductions of Late Permian and Triassic lineages were associated with decreases in the average level of tissue vascularization. Patterns in limb bone robusticity were less clear. As in the analyses of the raw data, phylogeny-corrected correlations between *RBT* and size or growth proxies were non-significant.

## Discussion

### General Histological Patterns

**Size, robusticity, and vascular growth proxies**—Biologically meaningful associations are detectable in therocephalian histology, as in some other therapsid groups. For example, vascular growth proxies were strongly positively correlated with size as larger-bodied species

typically exhibited greater overall tissue vascularity (e.g., *Lycosuchus*, scylacosaurids, *Moschorhinus*). Previous tests incorporating a large histologic sample of dicynodonts and other therapsids found similar correlations between raw vascular growth proxies and size (estimated from skull lengths), although tests on a subset of dicynodonts were only marginally significant and non-significant when independent contrasts were evaluated (Botha-Brink and Angielczyk, 2010). The new data agree with these earlier results ~~by large measure~~. However, the present analysis found a strongly positive correlation between size and both vascular growth proxies (%*CV* and *POD*) even when corrected for phylogeny. Prior analyses implementing phylogeny-independent contrasts on dicynodonts were unable to identify similar patterns, despite a significant correlation between the raw data (Botha-Brink and Angielczyk, 2010). Improved statistical results in this study are a likely consequence of sampling bones of particular types separately (rather than averaging vascularity across all bones) and using cross-sectional measurements from sampled bones as a size proxy (rather than representative skull lengths from specimens that were not sampled histologically). Tests on raw cortical thickness (*RBT*) in dicynodonts also showed no clear association with size or degree of vascularization as in the present study, even though a positive association with size was discovered when corrected for phylogeny. No correlation was observed between bone robusticity (*RBT*) and size or degree of vascularization in therocephalians (raw or phylogenetically-corrected), suggesting that bone robusticity is not necessarily tied directly to growth (perhaps being constrained by ecology, habitat, or mechanical regimen in different groups of therocephalians). Similarly, data on the genus *Moschorhinus* indicated that overall bone compactness was related to the thickness of the bone wall, but was largely independent of growth and degree of vascularity (Huttenlocker and Botha-Brink, 2013).

### Phylogenetic Patterns

Previous interpretations of growth patterns in early therocephalians were based on limited

information from incomplete specimens (Ricqlès, 1969; Ray, Botha & Chinsamy, 2004; Chinsamy-Turan and Ray, 2012). Additional specimens described here suggest that at least some large-bodied predators from the Middle Permian, including *Lycosuchus* and some scylacosaurids, exhibited subplexiform FLB in propodial elements. Some of the larger-bodied predators in the sample also showed the highest degree of cortical vascularization. This is remarkable, as subplexiform FLB is one of the most rapidly deposited tissue-types in archosaurian and mammalian limb bones, and similarly vascularized bone in birds and mammals forms periosteally at a rate generally greater than 15  $\mu\text{m}/\text{day}$  (Castanet et al., 2000; Margerie, Cubo & Castanet, 2002; Cubo et al., 2012). It is noteworthy that the subplexiform tissue complex, present in *Lycosuchus* and scylacosaurids, represents the prototype upon which earlier workers first described FLB [see Stein and Prondvai (2013) for a review]. This subplexiform condition is conspicuously lacking in the whaitsiid *Theriognathus* (Fig. 5) and some later eutheriocephalians. Consequently, the evolutionary scenario suggested by Ricqlès (1969) and critically re-examined by Chinsamy-Turan and Ray (2012) should be revised: basal therocephalians exhibited highly vascularized FLB and grew relatively rapidly over many growing seasons but with frequent interruptions, in contrast to some later eutheriocephalians (with the exception of the akidnognathid *Moschorhinus*, which maintained relatively fast growth).

Moreover, elevated vascularity and rapid growth may be a characteristic of larger bodied taxa, an interpretation that is supported by observations in other large predatory theriodonts such as the cynodont *Cynognathus* and some large gorgonopsians (Botha-Brink, Abdala & Chinsamy-Turan, 2012; Chinsamy-Turan and Ray, 2012). Importantly, evolutionary decreases in body size during the Permian (Huttenlocker, 2013 and [in press](#)) were associated with decreases in overall degree of skeletal vascularization. Both hofmeyriids and *Theriognathus* (in spite of its substantial size) showed modest cortical vascularity and smaller mean primary osteon diameters than in basal lycosuchids, scylacosaurids or akidnognathids, but the baurioids (which are deeply nested

in the tree and generally smaller-bodied) had the least vascularized bone tissues (Fig. 6). These clade-level patterns suggest that reductions in body size of some Late Permian eutheriocephalians were coupled with decreased rates of skeletal apposition leading up to the end-Permian extinction, particularly in the baurioid lineage.

## Growth and the End-Permian Extinction

The end-Permian extinction was associated with evidence of temporary body size reductions, restricted primarily to faunas of the earliest Triassic (Induan) (although size reductions in some therapsids may reflect larger-scale patterns of body size evolution tracing back to the Permian; Huttenlocker, 2013 and *in press*). Such size shifts have been documented previously based on invertebrate burrows, foraminifera, brachiopods, gastropods, bivalves, conodonts, and fish (Twitchett and Barras, 2004; Payne, 2005; Twitchett, 2007; Luo et al., 2008; Mutter and Neuman, 2009; Metcalfe, Twitchett & Price-Lloyd, 2011; Song, Tong & Chen, 2011; Rego et al., 2012). Nevertheless, questions remain regarding the evolution of growth patterns and their underlying influence on size shifts (Twitchett, 2007; Harries and Knorr, 2009). For example, organisms may have experienced slower overall growth rates in response to more limited resources or environmental degradation during the Permian-Triassic transition. Growth mark analyses on marine brachiopod shells (i.e., '*Lingula*') have indicated slow growth rates with frequent interruptions to growth in earliest Triassic shells (Metcalfe, Twitchett & Price-Lloyd, 2011). The authors attributed their results to suboptimal environmental conditions, including episodes of benthic hypoxia, hypercapnia, ocean acidification, and/or disruptions to primary productivity. Such environmental factors would place strong physiological limits on shell formation. However, identifications of lingulid specimens were tenuous given conservatism in external morphology of the group, and growth marks were only studied in shells from Triassic survival and recovery faunas without being compared to Permian specimens. Alternatively, surviving lineages could have exhibited heterochronic shifts shortening time to maturity (e.g.,

progenesis) and thus rapid, sustained growth over a brief growth period. Progenesis is a classic example of an *r*-selection strategy in perturbed or unstable environments (Gould, 1977) and has been identified as a potential mechanism of some Lilliput patterns (Harries, Kauffman & Hansen, 1996). Finally, if shifts in body size distributions were influenced primarily by differential extinction of large- versus small-bodied forms, then there may have been no resulting changes in growth patterns at all (that is to say, changes in growth dynamics are not necessary to explain post-extinction body size distributions).

**Growth patterns in Permo-Triassic therapsids compared**—New data on growth patterns in nonmammalian therapsids, as well as other Permo-Triassic tetrapods, offer the potential to further evaluate patterns of selectivity during mass extinctions (Botha-Brink and Angielczyk, 2010; Botha-Brink and Smith, 2012). Bone histology has been studied in numerous genera of Permian and Triassic dicynodont therapsids (Chinsamy and Rubidge, 1993; Ray, Botha & Chinsamy, 2004; Ray, Bandyopadhyay & Bhawal, 2009; Ray, Botha-Brink & Chinsamy-Turan, 2012) and recent progress in dicynodont paleobiology has permitted evolutionary investigations of their growth patterns (Botha-Brink and Angielczyk, 2010). Increased rates of skeletal growth originated relatively early, either within or prior to the divergence of bidentalian dicynodonts (e.g., *Dicynodon*, *Lystrosaurus*) by the early-Late Permian. Medium-to-large Late Permian dicynodonts continued to show patterns of increased cortical vascularity, especially within the Permo-Triassic boundary-crossing genus *Lystrosaurus*, which demonstrated some of the highest levels of tissue vascularity (~20%). Triassic specimens of *Lystrosaurus* showed relatively higher vascularity and fewer growth marks. In the therocephalian *Moschorhinus*, the only large therapsid predator to cross the Permian-Triassic boundary, within-lineage size reductions were associated with the maintenance of rapid but attenuating growth over a short period (Huttenlocker and Botha-Brink, 2013). This pattern suggests that *Moschorhinus* may have been under selection for reaching its adult size relatively more quickly than in other Permian

therocephalians. Notably, *Moschorhinus* exhibited comparably high levels of tissue vascularity as *Lystrosaurus* during the Triassic (~20-25%).

Whereas anecdotal evidence in *Lystrosaurus* and *Moschorhinus* is suggestive of within-lineage heterochronic shifts, clade-level patterns introduce a more complex explanation for observed body size reductions in therocephalians. In particular, body size reductions occurred early during the evolution of eutheriocephalians and were associated with a lesser degree of cortical vascularity in medium-to-small-bodied Permian forms (e.g., hofmeyriids and especially baurioids). The two major subclades of therocephalians that persisted into the earliest Triassic, Akidnognathidae and Baurioidea, revealed distinctly different growth patterns from each other as interpreted through their tissue texture and degree of vascularity. Their histology suggests a bimodality of life history strategies in earliest Triassic therocephalians: small-to-medium akidnognathids with well-vascularized (fast-growing) bone and smaller-bodied baurioids with less vascularized (slower-growing) bone. However, both groups shared a reduced number of growth marks compared to their Permian relatives in addition to their generally smaller sizes. This nuance is not evident from the quantitative analysis based on vascular proxies of growth rate alone, but is evident from growth mark counts in surveyed specimens. Permian theriodonts that have been sampled histologically, including some gorgonopsians, the cynodont *Procynosuchus*, basal therocephalians, Permian (but not Triassic) specimens of *Moschorhinus*, hofmeyriids, and *Theriongnathus*, typically showed evidence of prolonged, multi-year growth often to larger body sizes, a pattern that is not represented in earliest Triassic therapsids sampled to date (Botha-Brink and Angielczyk, 2010; Botha-Brink, Abdala & Chinsamy, 2012).

The present discussion of associations between micro- and macrostructure provides a more functional and wholistic context for the evolution of histological features in Permian and Triassic therocephalians. However, it is important to note that the patterns discussed here have not been evaluated quantitatively and therefore merit future investigation. Recent large-scale

phylogenetic studies in other therapsids have addressed how life history and functional morphology might have contributed to the success of some groups during the Late Permian and Triassic (e.g., bidentalian dicynodonts). For example, the degree of development of the secondary palate has been linked anecdotally to new environmental conditions with the onset of the Early Triassic, particularly a dramatic decline in atmospheric  $pO_2$  from the Late Permian and continuing through the Middle and Late Triassic (Retallack, 2003). However, a rigorous collections-based study found no difference between secondary palate length in Permian and Triassic dicynodonts when corrected for size and phylogeny (Angielczyk and Walsh, 2008). Similarly, a bony secondary palate can be found in a number of therocephalian subgroups, both in the Permian and Triassic, and Triassic therocephalian faunas consisted of species both with (e.g., baurioids) and without (e.g., akidnognathids) a secondary palate (Fig. 7). No clear association with global hypoxia and respiratory efficiency can be made based on this character, and, as a result, other factors may have been more important in maintaining and shaping the evolution of the secondary palate (e.g., feeding mechanics; Thomason and Russell, 1986).

Similar studies addressing the possible effects of hypoxia on cortical tissue vascularity have found few differences between Permian and Triassic therapsids, instead demonstrating that highly vascularized tissues with enlarged canals evolved early in bidentalian dicynodonts (Botha-Brink and Angielczyk, 2010). In therocephalians, variation in the degree of vascularization of limb cortices is best explained by size variation observed across clades (Fig. 7). Most smaller-bodied groups exhibited less vascularized limb bone cortices, a character that evolved relatively early in the evolutionary history of eutheriocephalians and held over in some small Triassic taxa. The smallest Triassic forms, derived baurioids, typically had lighter, more gracile skeletons with an open medullary cavity, thinner bone walls, and few to no growth marks. In addition to longer, more slender limb bones, they also had an elongate hind foot with a calcaneal tuber on the heel, maxillary bridge forming a bony secondary palate (discussed above), increasingly specialized



multi-cusped teeth, and often lacked a parietal foramen (or reduced the pineal body altogether as in *Tetracynodon*; Sigurdson et al., 2012). The selective value of maintaining a parietal eye for temperature regulation and modulating melatonin production may have been diminished in some small, nocturnal or crepuscular baurioid therocephalians, or in short-lived animals less dependent on seasonal cues in photoperiodicity (Roth, Roth & Hotton, 1986). The latter scenario is consistent with the lack of cyclic bone deposition and paucity of growth marks in small Triassic baurioids (although one genus, *Scaloposaurus*, is distinguished from other small Triassic baurioids in its retention of the parietal foramen and pineal body).

## Conclusion

A survey of histological patterns in therocephalians found that limb bone cortices composed of thick deposits of FLB with cyclic growth marks were widespread in early therocephalians, but evolutionary decreases in adult body sizes of some clades were associated with reductions in cortical vascularity and skeletal growth leading up to the end-Permian mass extinction. In Permo-Triassic therocephalians, a pattern of multi-year growth to large body size that was common in the Permian was selected against in the earliest Triassic. This conclusion is supported by (1) ecological removal of large-bodied taxa having prolonged, multi-year growth patterns; (2) cladistically inferred survival of small-bodied taxa with modest skeletal apposition rates, but truncated growth durations (i.e., baurioids); and (3) within-lineage shifts in growth patterns observed in boundary-crossing genera in the Karoo (i.e., *Lystrosaurus* and *Moschorhinus*). A synergistic combination of local within-lineage effects and differential extinction patterns strongly influenced Triassic Lilliput faunas, weakening the hypothesized role of rapid adaptive evolution of new small-bodied forms. Similar within-lineage size decreases and size selective extinctions contributed strongly to Lilliput patterns in marine gastropods,



foraminifera, and brachiopods, although all three mechanisms have been invoked to explain Early Triassic foraminifera size distributions globally (Payne, 2005; Metcalfe, Twitchett & Price-Lloyd, 2011; Song, Tong & Chen, 2011; Rego et al., 2012). Contrary to the present results, growth mark analyses on lingulid brachiopods are suggestive of different physical factors influencing skeletal growth in marine benthos (due to slowed, but prolonged shell secretion over many years) (Metcalfe, Twitchett & Price-Lloyd, 2011). More skeletochronologic and phylogenetic data are needed, however, to understand the generality of these patterns among Permo-Triassic Lilliput taxa in marine and terrestrial realms.

Although some effects on size and growth are observable in Triassic therocephalians (and perhaps therapsids more generally), it is important to note that much of the diversity observed in the earliest Triassic *Lystrosaurus* Assemblage Zone of the Karoo originated during the Late Permian, and that variation in body sizes and growth patterns during the Late Permian was supplanted by increased bimodality in the Early Triassic *Lystrosaurus* AZ: small-to-medium, fast-growing akidnognathids and the still smaller, slower-growing baurioids. Small size and short growth duration were dominant life history strategies of Early Triassic therocephalians in the Karoo, and reductions in size were typically associated with lesser tissue vascularity and growth rates across but not within taxa. Furthermore, although these strategies were apparently common in the post-extinction environment, their success was temporary. Low rates of origination in therocephalians during this time, coupled with small sizes and reduced niche occupation may have afforded the opportunity for more marginalized groups to diversify (e.g., cynodonts and archosauromorphs). Future applications of phylogenetic comparative methods to studies of body size and growth during the Permo-Triassic will enhance our understanding of interplay between macroevolution and extinctions, and will identify areas of phylogeny that correspond to shifts in trait evolution that conferred success on lineages.

## Acknowledgments

AKH thanks S. Herring, E. Nesbitt, C. Sidor, and G. Wilson for providing helpful suggestions on the project. F. Abdala and B. Rubidge (BP), E. Butler (NMQR), E. De Kock and J. Neveling (CGS), P. Holroyd (UCMP), and S. Kaal and R. Smith (SAM) are acknowledged for specimen access. F. Abdala and K. Angielczyk offered additional insights into body size evolution and growth, as well as therapsid diversity patterns during the end-Permian extinction. The National Museum preparatory staff also provided assistance and preparation of some specimens for histological processing: J. Nyaphuli, J. Mohoi, N. Ntheri, S. Stuurman, S. Ledibane, S. Chaka, and W. Molehe. Digital image processing and some histologic preparation performed by J. Lungmus (University of Washington). C. Organ and A. Crompton are acknowledged for their kind and constructive reviews of this manuscript.

## References

- Abdala F, Rubidge BS, van den Heever J. 2008. The oldest therocephalians (Therapsida, Eutheriodontia) and the early diversification of Therapsida. *Palaeontology* 51:1011–1024.
- Angielczyk KD, Walsh ML. 2008. Patterns in the evolution of nares size and secondary palate length in anomodont therapsids (Synapsida): implications for hypoxia as a cause of end-Permian tetrapod extinctions. *Journal of Paleontology* 82:528-542.
- Botha J. 2003. Biological aspects of the Permian dicynodont *Oudenodon* (Therapsida:Dicynodontia) deduced from bone histology and cross-sectional geometry. *Palaeontologia Africana* 39:37–44.
- Botha J, Angielczyk K. 2007. An integrative approach to distinguishing the Late Permian dicynodont species *Oudenodon baini* and *Tropidostoma microtrema* (Therapsida: Anomodontia). *Palaeontology* 50:1175–1209.

- 596 Botha J, Chinsamy A. 2000. Growth patterns deduced from the histology of the cynodonts  
597 *Diademodon* and *Cynognathus*. *Journal of Vertebrate Paleontology* 20:705–711.
- 598 Botha J, Chinsamy A. 2004. Growth and lifestyle adaptations of the Triassic non-mammalian  
599 cynodont *Trirachodon*. *Acta Palaeontologica Polonica* 49:619–627.
- 600 Botha J, Chinsamy A. 2005. Growth patterns of *Thrinaxodon*, a non-mammalian cynodont from the  
601 Early Triassic of South Africa. *Palaeontology* 48:385–394.
- 602 Botha J, Smith RMH. 2006. Rapid vertebrate recuperation in the Karoo Basin of South Africa  
603 following the end-Permian extinction. *Journal of African Earth Sciences* 45:502–514.
- 604 Botha-Brink J & al. 2012. The radiation and osteohistology of nonmammaliaform cynodonts.  
605 *Forerunners of Mammals: Radiation, Histology, Biology*, Indiana University Press,  
606 Bloomington, ed Chinsamy-Turan A, pp. 223–246.
- 607 Botha-Brink J, Angielczyk K. 2010. Do extraordinarily high growth rates in Permo-Triassic  
608 dicynodonts (Therapsida, Anomodontia) explain their success before and after the end-  
609 Permian extinction? *Zoological Journal of the Linnean Society* 160:341–365.
- 610 Botha-Brink J, Smith RMH. 2012. Osteohistology of the Triassic archosauromorphs *Prolacerta*,  
611 *Proterosuchus*, *Euparkeria*, and *Erythrosuchus* from the Karoo Basin of South Africa.  
612 *Journal of Vertebrate Paleontology* 31:1238–1254.
- 613 Buffrénil V de & al. 2007. Bone vascular supply in monitor lizards (Squamata: Varanidae):  
614 implications of size, growth, and phylogeny. *Journal of Morphology* 269:533–543.
- Calder WA III. 1984. *Size, Function, and Life History*. Harvard University Press, Cambridge: 431 pp.
- 615 Case TJ. 1978. On the evolution and adaptive significance of postnatal growth rates in the  
616 terrestrial vertebrates. *The Quarterly Review of Biology* 53:243–282.
- Castanet J & al. 2000. Periosteal bone growth rates in extant ratites (ostrich and emu): implications for assessing  
growth in dinosaurs. *Comptes Rendus de l'Académie des Sciences de Paris, Science de la Vie* 323:543–550.
- 617 Chinsamy A. 1993. Bone histology and growth trajectory of the prosauropod dinosaur

- 618 *Massospondylus carinatus* Owen. *Modern Geology* 18:319–329.
- 619 Chinsamy A, Abdala F. 2008. Paleobiological implications of the bone microstructure of South  
620 American traversodontids (Therapsida: Cynodontia). *South African Journal of Science*  
621 104:225–230.
- 622 Chinsamy A, Hurum J. 2006. Bone microstructure and growth patterns of early mammals. *Acta*  
623 *Palaeontologica Polonica* 51:325–338.
- 624 Chinsamy A, Raath M. 1992. Preparation of fossil bone for histological examination. *Palaeontologia*  
625 *Africana* 29:39–44.
- 626 Chinsamy A, Rubidge BS. 1993. Dicynodont (Therapsida) bone histology: Phylogenetic and  
627 physiological implications. *Palaeontologia Africana* 30:97–102.
- Chinsamy-Turan A. 2012. *Forerunners of Mammals: Radiation, Histology, Biology*. Indiana University Press,  
Bloomington.
- 628 Chinsamy-Turan A, Ray S. 2012. Bone histology of some therocephalians and gorgonopsians, and  
629 evidence of bone degradation by fungi. *Forerunners of Mammals: Radiation, Histology,*  
630 *Biology*, Indiana University Press, Bloomington, ed Chinsamy-Turan A, pp. 199–221.
- 631 Cormack D. 1987. *Ham's Histology*. Lippincott, New York, 732 pp.
- 632 Cubo, J & al. 2012. Paleohistological estimation of bone growth rate in extinct archosaurs.  
633 *Paleobiology* 38:335–349.
- 634 Currey JD. 1987. The evolution of the mechanical properties of amniote bone. *Journal of*  
635 *Biomechanics* 20:1035–1044.
- 636 Currey JD. 2002. *Bones: Structure and Mechanics, 2nd ed*. Princeton University Press, Princeton,  
637 N.J.
- 638 Currey JD, Alexander RMcN. 1985. The thickness of the walls of tubular bones. *Journal of Zoology*  
639 206:453–468.
- 640 Díaz-Uriarte R, Garland T. 1996. Testing hypotheses of correlated evolution using

- 641 phylogenetically independent contrasts: sensitivity to deviations from Brownian motion.
- 642 *Systematic Biology* 45:27–47.
- 643 Enlow DH. 1969. The bone of reptiles. *Biology of the Reptilia, Volume 1: Morphology A*,
- 644 Academic Press, London, eds Gans C, Bellairs A, & Parsons T, pp. 45-77.
- 645 Enlow DH, Brown SO. 1957. A comparative histological study of fossil and Recent bone tissues, Part
- 646 II. *Texas Journal of Science* 9:186–214.
- 647 Erickson G & al. 2004. Gigantism and comparative life-history parameters of tyrannosaurid
- 648 dinosaurs. *Nature* 430:772–775.
- 649 Felsenstein J. 1985. Phylogenies and the comparative method. *American Naturalist* 125:1–15.
- 650 Fourie H, Rubidge BS. 2007. The postcranial skeletal anatomy of the therocephalian *Regisaurus*
- 651 (Therapsida: Regisauridae) and its utilization for biostratigraphic correlation.
- 652 *Palaeontologia Africana* 42:1–16.
- 653 Fourie H, Rubidge BS. 2009. The postcranial skeleton of the basal therocephalian *Glanosuchus*
- 654 *macrops* (Scylacosauridae) and comparison of morphological and phylogenetic trends
- 655 amongst the Theriodontia. *Palaeontologia Africana* 44:27–39.
- 656 Garland T & al. 2005. Phylogenetic approaches in comparative physiology. *Journal of*
- 657 *Experimental Biology* 208:3015–3035.
- 658 Germain D, Laurin M. 2005. Microanatomy of the radius and lifestyle in amniotes (Vertebrata,
- 659 Tetrapoda). *Zoologica Scripta* 34:335–350.
- 660 Gould SJ. 1977. *Ontogeny and Phylogeny*. Belknap Press of Harvard University Press, Cambridge.
- 661 Green JL & al. 2010. Limb bone histology and growth in *Placerias hesternus* (Therapsida:
- 662 Anomodontia) from the Upper Triassic of North America. *Palaeontology* 53:347–364.
- 663 Harries PJ, Kauffman EG, Hansen TA. 1996. Models of biotic survival following mass extinction.
- 664 *Biotic Recovery from Mass Extinction Events. Geological Society of London Special*
- 665 *Publication* 102, ed Hart MB, pp. 41–60.

- 666 Harries PJ, Knorr PO. 2009. What does the ‘Lilliput Effect’ mean? *Palaeogeography,*  
667 *Palaeoclimatology, and Palaeoecology* 284:4–10.
- 668 Huttenlocker AK. 2009. An investigation into the cladistic relationships and monophyly of  
669 therocephalian therapsids (Amniota: Synapsida). *Zoological Journal of the Linnean*  
670 *Society* 157:865–891.
- 671 Huttenlocker AK. 2013. *The Paleobiology of South African Therocephalian Therapsids*  
672 *(Amniota, Synapsida) and the Effects of the End-Permian Extinction on Size, Growth, and*  
673 *Bone Microstructure*. Unpublished PhD dissertation. University of Washington, Seattle.  
674 414 p.
- Huttenlocker AK (in press for 2014) Body size reductions in nonmammalian eutheriodont therapsids (Synapsida)  
during the end-Permian mass extinction. *PLOS:ONE*. DOI: 10.1371/journal.pone.0087553
- Huttenlocker AK, Botha-Brink J. 2013. Body size and growth patterns in the therocephalian *Moschorhinus kitchingi*  
(Therapsida: Eutheriodontia) before and after the end-Permian extinction in South Africa. *Paleobiology*  
39:253–277.
- 675 Huttenlocker AK & al. 2011. Comparative osteohistology of hyperelongate neural spines in the  
676 Edaphosauridae (Amniota: Synapsida). *Palaeontology* 54:573–590.
- 677 Huttenlocker AK, Rega E. 2012. The paleobiology and bone microstructure of pelycosaurian-  
678 grade synapsids. *Forerunners of Mammals: Radiation, Histology, Biology*, Indiana  
679 University Press, Bloomington, ed Chinsamy-Turan A, pp. 90–119.
- 680 Huttenlocker AK & al. 2010. Comparative anatomy and osteohistology of hyperelongate neural  
681 spines in the sphenacodontids *Sphenacodon* and *Dimetrodon* (Amniota: Synapsida).  
682 *Journal of Morphology* 271:1407–1421.
- 683 Huttenlocker AK & al. 2011. A new specimen of *Promoschorhynchus* (Therapsida:  
684 Therocephalia: Akidnognathidae) from the Lower Triassic of South Africa and its  
685 implications for theriodont survivorship across the Permo-Triassic boundary. *Journal of*

- 686       *Vertebrate Paleontology* 31:405–421.
- 687   Huttenlocker, A., H. N. Woodward, B. K. Hall. 2013. Chapter 2: Biology of Bone. *Bone*
- 688       *Histology of Fossil Tetrapods: Advancing Methods, Analysis, and Interpretation*,
- 689       University of California Press, Berkeley, eds Padian K & Lamm E-T, pp. 12–34.
- 690   Jasinoski SC & al. 2010. Functional implications of dicynodont cranial suture morphology.
- 691       *Journal of Morphology* 271:705–728.
- 692   Kemp TS. 1972a. Whaitsiid Therocephalia and the origin of cynodonts. *Philosophical*
- 693       *Transactions of the Royal Society of London: Series B* 264:1-54.
- 694   Kemp TS. 1972b. The jaw articulation and musculature of the whaitsiid Therocephalia. *Studies in*
- 695       *Vertebrate Evolution*, Winchester Press, New York, eds Joysey KA & Kemp TS, pp. 213-
- 696       230.
- 697   Kemp TS. 1978. Stance and gait in the hindlimb of a therocephalian mammal-like reptile.
- 698       *Journal of Zoology* 186:143–161.
- 699   Kemp TS. 1986. The skeleton of a baurioid therocephalian therapsid from the Lower Triassic
- 700       (*Lystrosaurus* Zone) of South Africa. *Journal of Vertebrate Paleontology* 6:215–232.
- 701   Kriloff A & al. 2008. Evolution of bone microanatomy of the tetrapod tibia and its use in
- 702       paleobiological inference. *Journal of Evolutionary Biology* 21:807–826.
- 703   Laurin M & al. 2004. The evolution of long bone microstructure and lifestyle in lissamphibians.
- 704       *Paleobiology* 30:589–613.
- 705   Lee AH. 2007. *Interplay Between Growth and Mechanics in the Evolution of Bone*
- 706       *Microstructure in Dinosaurs*. Unpublished Ph.D. dissertation. University of California,
- 707       Berkeley: 210 pp.
- 708   Lee AH & al. 2013. Chapter 8: Analysis of growth rates. *Bone Histology of Fossil Tetrapods:*
- 709       *Advancing Methods, Analysis, and Interpretation*, University of California Press,
- 710       Berkeley, eds Padian K & Lamm E-T, pp. 209–243.



Luo G & al. 2008. Size variation of conodont elements of the *Hindeodus-Isarcicella* clade during the Permian-Triassic transition in South China and its implications for mass extinction. *Palaeogeography, Palaeoclimatology, Palaeoecology* 264:176–187.

Maddison WP, Maddison DR. 2007. Mesquite: a modular system for evolutionary analysis. Version 2.0.  
<http://mesquiteproject.org>

711 Margerie E de & al. 2002. **Bone typology and growth rate: testing and quantifying ‘Amprino’s**  
712 **rule’ in the mallard (*Anas platyrhynchos*). *Comptes Rendus Biologies* 325:221–230.**

Margerie E de & al. 2004. Assessing a relationship between bone microstructure and growth rate: a fluorescent labeling study in the king penguin chick (*Aptenodytes patagonicus*). *Journal of Experimental Biology* 207:869–879.

713 Metcalfe B & al. 2011. Size and growth rate of ‘Lilliput’ animals in the earliest Triassic.  
714 *Palaeogeography, Palaeoclimatology, Palaeoecology* 308:171–180.

715 Midford PE, Garland T, & Maddison WP. 2011. PDAP:PDTree module for Mesquite (version  
716 1.16). [http://mesquiteproject.org/pdap\\_mesquite/index.html](http://mesquiteproject.org/pdap_mesquite/index.html).

717 Mutter RJ, Neuman AG. 2009. Recovery from the end-Permian extinction event: evidence from  
718 “Lilliput *Listracanthus*.” *Palaeogeography, Palaeoclimatology, Palaeoecology* 284:22–28.

Nasterlack T & al. 2012. New insights into the biology of the Permian genus *Cistecephalus* (Therapsida, Dicynodontia). *Journal of Vertebrate Paleontology* 32:1396–1410.

Payne JL. 2005. Evolutionary dynamics of gastropod size across the end-Permian extinction and through the Triassic recovery interval. *Paleobiology* 31:269–290.

Peters R. 1983. *The Ecological Implications of Body Size*. Cambridge University Press, Cambridge: 344 pp.

Rasband WS. *ImageJ*, U. S. National Institutes of Health, Bethesda, Maryland, USA, <http://imagej.nih.gov/ij/>, 1997-2012.

719 Ray S & al. 2004. Bone histology and growth patterns of some nonmammalian therapsids. *Journal of*  
720 *Vertebrate Paleontology* 24:634–648.

721 Ray S & al. 2005. *Lystrosaurus murrayi* (Therapsida; Dicynodontia): bone histology, growth and  
722 lifestyle adaptations. *Palaeontology* 48:1169–1185.



- 723 Ray S & al. 2009. Growth patterns as deduced from bone microstructure of some selected  
724 neotherapsids with special emphasis on dicynodonts: Phylogenetic implications.  
725 *Palaeoworld* 18:53–66.
- 726 Ray S & al. 2010. Chapter 5: Bone histology of a kannemeyriid dicynodont *Wadiasaurus*:  
727 palaeobiological implications. *New Aspects of Mesozoic Biodiversity (Lecture Notes in Earth*  
728 *Sciences 132)* Springer, Berlin, ed Bandyopadhyay S, pp. 73–89.
- 729 Ray S & al. 2012. Dicynodont growth dynamics and lifestyle adaptations. *Forerunners of*  
730 *Mammals: Radiation, Histology, Biology*, Indiana University Press, Bloomington, ed  
731 Chinsamy-Turan A, pp. 121–146.
- 732 Ray S, Chinsamy A. 2004. *Diictodon feliceps* (Therapsida, Dicynodontia): bone histology, growth  
733 and biomechanics. *Journal of Vertebrate Paleontology* 24:180–194.
- Rego BL & al. 2012. Within- and among-genus components of foraminiferan size evolution during mass extinction,  
recovery, and background intervals. *Paleobiology* 38:627–643.
- Retallack GJ. 2003. Vertebrate extinction across the Permian-Triassic boundary in the Karoo Basin of South Africa.  
*Bulletin of the Geological Society of America* 115:1133–1152.
- 734 Ricqlès A de. 1969. Recherches paléohistologiques sur les os longs des Tétrapodes II—Quelques  
735 observations sur la structure des os longs des Thériodontes. *Annales de Paléontologie*  
736 *(Vertébrés)* 55:1–52. [in French]
- 737 Ricqlès A de. 1974a. Evolution of endothermy: histological evidence. *Evolutionary Theory* 1:51–80.
- 738 Ricqlès A de. 1974b. Recherches paléohistologiques sur les os longs des Tétrapodes IV—  
739 Eothériodontes et pélycosaures. *Annales de Paléontologie (Vertébrés)* 60:3–39. [in  
740 French]
- 741 Ricqlès A de. 1976. On bone histology of fossil and living reptiles, with comments on its functional  
742 and evolutionary significance. *Morphology and Biology of Reptiles*, Academic Press,  
743 London, eds Bellairs A & Cox CB, pp.123–150.

- 744 Roth, JJ & al. 1986. The parietal foramen and eye: their function and fate in therapsids. *The Ecology*  
745 *and Biology of Mammal-like Reptiles*. Smithsonian Institution Press, Washington, D.C., eds  
746 Hotton N, MacLean PD, Roth JJ, & Roth EC, pp. 173–184.
- 747 Shelton CD & al. 2013. Long bone histology indicates sympatric species of Dimetrodon (Lower  
748 Permian, Sphenacodontidae). *Earth and Environmental Science Transactions of the Royal*  
749 *Society of Edinburgh* 103:1–20.
- 750 Sigurdson T. 2006. New features of the snout and orbit of a therocephalian therapsid from South  
751 Africa. *Acta Palaeontologica Polonica* 51:63–75.
- 752 Sigurdson T & al. 2012. Reassessment of the morphology and paleobiology of the therocephalian *Tetracynodon darti*  
(Therapsida), and the phylogenetic relationships of Baurioidea. *Journal of Vertebrate Paleontology*  
32:1113–1134.
- 753 Smith RMH, Botha J. 2005. The recovery of terrestrial vertebrate diversity in the South African  
Karoo Basin after the end-Permian extinction. *Comptes Rendus Palevol* 4:623–636.
- 754 Song H & al. 2011. Evolutionary dynamics of the Permian-Triassic foraminifer size: Evidence for Lilliput effect in  
the end-Permian mass extinction and its aftermath. *Palaeogeography, Palaeoclimatology, Palaeoecology*  
308:98–110.
- 755 Stearns SC. 1992. *The Evolution of Life Histories*. Oxford University Press, Oxford: 249 pp.
- 756 Stein K, Prondvai E. 2013. Rethinking the nature of fibrolamellar bone: an integrative biological  
revision of sauropod plexiform bone formation. *Biological Reviews of the Cambridge*  
*Philosophical Society* 2013. doi: 10.1111/brv.12041
- 757 Thomason JJ, Russell AP. 1986. Mechanical factors in the evolution of the mammalian secondary  
758 palate: a theoretical analysis. *Journal of Morphology* 189:199–213.
- 759 Twitchett RJ. 2007. The Lilliput effect in the aftermath of the end-Permian extinction event.  
760 *Palaeogeography, Palaeoclimatology, Palaeoecology* 252:132–144.
- 761 Twitchett RJ, Barras CG. 2004. Trace fossils in the aftermath of mass extinction events. *The*  
762 *Application of Ichnology to Palaeoenvironmental and Stratigraphic Analysis, Geological*

*Society Special Publications 228*, Geological Society of London, London, ed McIlroy D, pp. 397-418.

Urbanek A. 1993. Biotic crises in the history of Upper Silurian graptoloids: a paleobiological model. *Historical Biology* 7:29–50.

Wall PW. 1983. The correlation between high limb-bone density and aquatic habitats in recent mammals. *Journal of Paleontology* 57:197–207.

Wilson JW. 1994. Histological techniques. *Vertebrate Paleontological Techniques* Cambridge University Press, New York, ed Leiggi P & May P, pp. 205–234.

**Appendix 1.** List of institutional abbreviations.

**BP**, Evolutionary Studies Institute (previously Bernard Price Institute for Palaeontological Research), University of Witwatersrand, Johannesburg; **CGS**, Council for Geoscience, Pretoria (former Geological Survey field numbers); **NMQR**, National Museum, Bloemfontein; **SAM**, Iziko South African Museum, Cape Town; **UCMP**, University of California Museum of Paleontology, Berkeley.

788  
789  
790  
791  
792  
793  
794  
795  
796  
797  
798  
799  
800

# **801 Tables & Figure Captions**

802 **Table 1.** Specimens, elements, and histometric measurements in studied therocephalians.

803

804 **Table 2.** Pearson's product-moment correlation statistics (Pearson's  $r$  and  $p$ ) for  
805 size, robusticity, and vascular growth proxies in therocephalians.

806

807 **Figure 1.** Stratigraphic ranges of therocephalians sampled histologically in the present study.

808 Dashed line indicates position of Permian-Triassic Boundary (PTB). Abbreviations: Chx,

809 Changxingian; *Cisteceph* AZ, *Cistecephalus* Assemblage Zone; *Cyn* sub A, *Cynognathus* subzone

810 A; *Eodicyno* AZ, *Eodicynodon* Assemblage Zone; Ind, Induan; Olen, Olenekian; *Pristerog* AZ,

811 *Pristerognathus* Assemblage Zone; Roa, Roadian; *Tapinoceph* AZ, *Tapinocephalus* Assemblage

812 Zone; *Tropido* AZ, *Tropidostoma* Assemblage Zone; Wor, Wordian.

813

814 **Figure 2.** Bone microstructure in selected basal therocephalians and Permo-Triassic

815 eutheriocephalians. **A**, Middle Permian *Lycosuchus* (SAM-PK-K9012), femur midshaft, dorsal

cortex showing subplexiform fibrolamellar bone viewed under non-polarized light. **B**, Middle Permian *Lycosuchus* (SAM-PK-9084), ulna midshaft, cortical fibrolamellar bone viewed at high magnification showing reticular canals in a woven-fibered matrix (crossed-nicols with wave plate). **C**, Scylacosauridae indet. (CGS R300), humerus midshaft, cortex viewed at low magnification showing growth marks (crossed-nicols with wave plate). **D**, Early Triassic akidnognathid *Olivierosuchus* (NMQR 3605), humerus midshaft, cortical fibrolamellar bone showing thick zone of reticular fibrolamellar bone followed by parallel-fibered bone and a LAG (crossed-nicols with wave plate). **E**, *Olivierosuchus* (SAM-PK-K10617), femur midshaft, close-up of primary osteons and woven-fibered interstitial matrix (crossed-nicols with wave plate). **F**, Late Permian hofmeyriid *Mirotenthes* (SAM-PK-K6511), femur midshaft, cortical parallel-fibered bone showing annular growth marks (crossed-nicols with wave plate). **G**, Late Permian whaitsiid *Theriognathus* (NMQR 3375), femur midshaft, cortical fibrolamellar bone viewed at medium magnification showing growth marks (non-polarized light). Arrows denote growth marks. Detailed descriptions and photomicrographs are provided in the Supporting Data file. Abbreviations: pfb, parallel-fibered bone; po, primary osteon; re, reticular fibrolamellar bone.

**Figure 3.** Bone microstructure in selected Permo-Triassic baurioid euterocephalians. **A**, Late Permian *Ictidosuchoides* subadult (SAM-PK-8659), radius midshaft, cortex and inner cancellous bony scaffold (crossed-nicols with wave plate). **B**, *Ictidosuchoides* adult (BP/1/4092), humerus midshaft, cortex with longitudinal and reticular primary osteons and growth marks (crossed-nicols with wave plate). **C**, Early Triassic *Tetracynodon* (NMQR 3745), humerus midshaft, cortex showing inner fibrolamellar bone and sparsely vascularized outer parallel-fibered bone (crossed-nicols with wave plate). **D**, Early Triassic *Scaloposaurus* (SAM-PK-K4638), humerus midshaft, cortex showing longitudinal and reticular fibrolamellar bone deposition followed by a thin collar of lamellar bone in the subperiosteal region (crossed-nicols with wave plate). **E**, Middle Triassic bauriid *Microgomphodon* (NMQR 3605), humerus midshaft, cortex showing reticular fibrolamellar bone with no growth marks (crossed-nicols with wave plate). **F**, *Microgomphodon* (NMQR 3605), femur midshaft, cortex showing reticular fibrolamellar bone (crossed-nicols with wave plate). Arrows denote growth marks. Detailed descriptions and photomicrographs are provided in the Supporting Data file. Abbreviations: pfb, parallel-fibered bone; re, reticular fibrolamellar bone.

**Figure 4.** Linear regression of vascular growth proxies against size (midshaft cross-sectional

area) from limb bone elements. **A**, Mean cortical vascularity (%*CV*) against midshaft cross-sectional area. **B**, Mean primary osteon diameter (*POD*) against midshaft cross-sectional area. **C**, mean %*CV* against mean *POD*. All correlations between vascular growth proxies and size are strongly positively correlated for both propodials (solid regression line) and epipodials (dashed regression line) (see statistical results in Table 2). Blue circles = propodials. Red circles = epipodials.

**Figure 5.** Comparison of bone histology and microvasculature in Permian *Theriongnathus* and *Moschorhinus*. **A**, *Theriongnathus* (NMQR 3375) femur midshaft cortex (non-polarized light). **B**, *Moschorhinus* (NMQR 3939) humerus midshaft cortex (non-polarized light). Note the greater overall degree of vascularity in ‘B.’

**Figure 6.** Mirror phylogenies of Permo-Triassic therocephalians sampled for bone histology (scaled to geologic time). Phylogenetic character mapping of histological traits estimated from propodials (left) and epipodials (right) reveals comparable ancestor-descendant changes for each pool of skeletal elements. **A**, average cortical vascularity (%*CV*). **B**, average primary osteon diameter (*POD*). **C**, relative bone wall thickness (*RBT*). Ancestral states were reconstructed using squared-change parsimony in Mesquite version 2.0 (Maddison and Maddison, 2007).

**Figure 7.** Summary of evolution of size and bone microstructural traits. Black bars represent stratigraphic ranges of taxa that were sampled histologically. Numbers in parentheses to right of black bars denote maximum size of taxon in interval of first appearance. Tree topology and ranges from Huttenlocker, 2013 and [in press](#). In graph at top of figure, circles represent average %*CV* and squares average *POD* of propodials (blue) and epipodials (red). Abbreviations: Chx, Changxingian; *Cisteceph* AZ, *Cistecephalus* Assemblage Zone; *Cyn* sub A, *Cynognathus* subzone A; *Eodicyno* AZ, *Eodicynodon* Assemblage Zone; Ind, Induan; Olen, Olenekian; *Pristerog* AZ, *Pristerognathus* Assemblage Zone; Roa, Roadian; *Tapinoceph* AZ, *Tapinocephalus* Assemblage Zone; *Tropido* AZ, *Tropidostoma* Assemblage Zone; Wor, Wordian.

# Table 1 (on next page)

Specimens, elements, and histometric measurements in studied therocephalians.

**Table 1.** Specimens, elements, and histometric measurements in studied therocephalians.

	% Largest*	Element	Midshaft cross-sectional area (mm <sup>2</sup> )	RBT (%)	K	Cortical vascularity (%)	Mean POD (μm)
<i>Lycosuchus</i>							
SAM-PK-9084	100%	radius	296.76	16	0.42	10.7[5.5]	101[11]
		ulna	325.40	25	0.38	15.7[2.0]	109[26]
SAM-PK-K9012	--	femur	1276.60	15	0.67	16.9[6.2]	168[17]
<i>Glanosuchus</i>							
BP/1/6228	47%	ulna	57.62	20	0.42	04.9[0.9]	51[13]
<i>Scylacosauridae</i> indet.							
BP/1/5576	--	radius	30.99	19	0.47	10.3[2.2]	68[10]
		ulna	36.63	24	0.53	09.7[4.3]	71[08]
BP/1/5587	--	humerus	169.42	33	0.29	13.3[3.2]	75[08]
		radius	88.26	23	0.46	03.5[0.7]	71[15]
		ulna	120.25	24	0.44	06.0[0.8]	85[07]
CGS R300	--	humerus	308.56	31	0.32	15.9[6.5]	112[13]
SAM-PK-5018	--	humerus	--	--	--	--	--
		radius	--	17	--	--	--
		femur	--	15	--	--	--
		tibia	83.86	24	0.60	10.3[1.5]	55[10]
		fibula	--	--	--	--	--
SAM-PK-11557	--	fibula	49.10	25	0.47	07.0[2.8]	44[07]
<i>Moschorhinus</i>							
NMQR 48	62%	humerus	205.85	30	0.45	16.6[5.0]	--
		radius	48.10	26	0.40	05.2[2.4]	67[18]
		ulna	102.67	27	0.43	04.8[1.3]	67[10]
		femur	263.13	22	0.58	12.8[4.8]	95[13]
NMQR 3939	65%	humerus	212.25	35	0.38	20.1[6.9]	134[36]
		radius	92.77	34	0.31	11.4[2.6]	101[18]
		ulna	101.86	29	0.44	10.1[2.1]	120[27]
		femur	206.82	28	0.44	18.4[6.9]	140[32]
		tibia (l)	103.85	37	0.30	15.5[1.9]	117[17]
		tibia (r)	114.28	31	0.39	15.6[5.8]	119[34]
NMQR 1640a	(84%)	femur	325.70	25	0.50	11.1[4.8]	96[12]
NMQR 1640b	--	tibia	427.87	35	0.39	09.7[2.5]	106[23]
NMQR 3351	91%	femur	488.65	21	0.55	13.6[5.0]	100[22]
NMQR 3684	(95%)	femur	378.12	27	0.53	14.2[4.6]	92[17]
SAM-PK-K118	59%	humerus	161.60	28	0.41	25.5[4.9]	100[17]
		radius	62.80	23	0.54	19.5[3.2]	101[17]
SAM-PK-K9953	59%	femur	155.13	25	0.42	20.9[5.8]	108[15]
UCMP 42787	(67%)	humerus	209.64	35	0.34	19.5[4.0]	107[20]
		radius	83.64	35	0.27	12.4[3.6]	92[18]
		fibula	42.53	32	0.28	10.8[1.9]	58[14]
BP/1/4227	76%	humerus	312.00	33	0.35	12.1[2.9]	100[16]
		radius	103.60	30	0.36	10.9[2.1]	88[10]
		ulna	96.00	26	0.48	08.5[2.0]	91[19]



**Table 1.** (Continued)

<i>Olivierosuchus</i>								
NMQR 3605	100%	humerus	47.54	36	0.38	09.9[1.8]	99[10]	
SAM-PK-K10617	(65%)	femur	23.72	19	0.65	03.4[1.1]	75[10]	
<i>Hofmeyria</i>								
BP/1/4404	69%	humerus	12.56	31	0.32	07.5[1.4]	72[11]	
		radius (l)	4.80	35	0.26	03.4[1.0]	46[05]	
		radius (r)	4.04	40	0.15	04.8[1.9]	47[05]	
		ulna (l)	3.63	39	0.22	03.0[0.6]	39[05]	
		ulna (r)	4.30	39	0.20	04.7[1.1]	43[08]	
<i>Mirotenthes</i>								
SAM-PK-K6511	78%	humerus	17.12	32	0.31	05.4[1.5]	54[07]	
		radius	6.28	34	0.33	03.5[1.5]	38[07]	
		ulna	5.24	32	0.42	02.0[0.5]	41[07]	
		femur	19.40	25	0.42	03.6[0.6]	58[07]	
		tibia	11.28	31	0.31	03.1[0.8]	38[06]	
		fibula	3.64	32	0.39	03.9[1.1]	32[04]	
<i>Theriongnathus</i>								
NMQR 3375	38%	femur	43.45	24	0.51	06.2[2.0]	65[10]	
BP/1/719	(62%)	femur	140.21	20	0.59	06.8[1.4]	87[11]	
<i>Ictidosuchoides</i>								
SAM-PK-K8659	50%	humerus	23.92	22	0.56	07.3[2.0]	45[05]	
		radius	10.08	24	0.52	04.2[1.1]	38[05]	
		femur	45.64	--	--	--	38[05]	
		tibia	28.32	16	0.63	02.8[1.0]	43[08]	
		fibula	10.44	22	0.59	03.8[1.5]	40[07]	
SAM-PK-K10423	(50%)	femur	34.80	14	0.71	04.7[1.8]	65[08]	
		tibia	9.52	23	0.49	04.3[1.5]	39[05]	
		fibula	19.60	19	0.47	04.7[1.6]	40[08]	
BP/1/75	--	humerus	44.27	19	0.64	11.1[1.4]	52[06]	
BP/1/4092	100%	humerus	60.19	22	0.56	10.2[2.1]	60[07]	
		radius	39.52	21	0.58	11.1[3.1]	62[08]	
		ulna	74.67	26	0.54	08.3[2.1]	52[08]	
<i>Tetracynodon</i>								
NMQR 3745	85%	humerus	11.44	22	0.56	8.1[3.2]	36[10]	
UCMP 78395	(94%)	humerus	16.48	24	0.49	4.9[1.7]	42[05]	
		radius	8.40	27	0.43	1.9[0.5]	42[10]	
		ulna	6.12	31	0.33	2.8[1.0]	38[06]	
		femur	18.28	17	0.66	5.0[2.5]	39[06]	
		tibia	12.48	25	0.48	3.9[0.7]	42[06]	
UCMP 78396	(94%)	humerus	16.96	21	0.54	4.7[1.9]	42[12]	
		femur	18.16	17	0.62	4.3[1.1]	42[07]	
		fibula	5.19	25	0.53	2.3[0.5]	35[06]	
<i>Scaloposaurus</i>								
SAM-PK-K4638	67%	humerus	15.34	--	--	06.6[1.6]	62[08]	

**Table 1.** (Continued)

<i>Microgomphodon</i>							
NMQR 3189	(82%)	humerus	11.04	21	0.61	08.8[2.1]	43[08]
		femur	16.52	18	0.61	06.1[1.6]	44[08]
		tibia	7.86	24	0.51	08.0[3.2]	41[09]
		fibula	3.33	29	0.39	04.2[0.9]	32[04]

\*Based on relative basal skull length (BSL). Parentheses indicate estimates for incomplete skulls.

## Table 2<sub>(on next page)</sub>

Pearson's product-moment correlation statistics (Pearson's  $r$  and  $p$ ) for size, robusticity, and vascular growth proxies in therocephalians.

**Table 2.** Pearson's product-moment correlation statistics (Pearson's  $r$  and  $p$ ) for size, robusticity, and vascular growth proxies in therocephalians.

	Propodial-only		Epipodial-only		Pooled	
	$r$	$p^*$	$r$	$p$	$r$	$p$
All therocephalians, raw data						
<i>ln midshaft area vs. RBT</i>	0.309	0.109	-0.186	0.267	-0.126	0.301
<i>ln midshaft area vs. %CV</i>	<b>0.744</b>	<b>&lt;0.001</b>	<b>0.714</b>	<b>&lt;0.001</b>	<b>0.746</b>	<b>&lt;0.001</b>
<i>ln midshaft area vs. POD</i>	<b>0.853</b>	<b>&lt;0.001</b>	<b>0.847</b>	<b>&lt;0.001</b>	<b>0.850</b>	<b>&lt;0.001</b>
<i>RBT vs. %CV</i>	<b>0.452</b>	<b>0.012</b>	0.034	0.839	0.149	0.217
<i>RBT vs. POD</i>	<b>0.360</b>	<b>0.050</b>	0.111	0.512	0.143	0.237
<i>%CV vs. POD</i>	<b>0.760</b>	<b>&lt;0.001</b>	<b>0.802</b>	<b>&lt;0.001</b>	<b>0.796</b>	<b>&lt;0.001</b>
All therocephalians, independent contrasts						
<i>ln midshaft area vs. RBT</i>	-0.466	0.174	-0.476	0.232	--	--
<i>ln midshaft area vs. %CV</i>	<b>0.765</b>	<b>0.006</b>	<b>0.807</b>	<b>0.015</b>	--	--
<i>ln midshaft area vs. POD</i>	<b>0.656</b>	<b>0.028</b>	<b>0.859</b>	<b>0.006</b>	--	--
<i>RBT vs. %CV</i>	-0.077	0.831	-0.224	0.592	--	--
<i>RBT vs. POD</i>	-0.472	0.168	-0.010	0.979	--	--
<i>%CV vs. POD</i>	<b>0.639</b>	<b>0.034</b>	<b>0.877</b>	<b>0.004</b>	--	--

\* $r$  and  $p$ -values in boldface are significant at  $\alpha = 0.05$

# Figure 1

Stratigraphic ranges of therocephalians sampled histologically in the present study.

Dashed line indicates position of Permian-Triassic Boundary (PTB). Abbreviations: Chx, Changxingian; *Cisteceph* AZ, *Cistecephalus* Assemblage Zone; *Cyn* sub A, *Cynognathus* subzone A; *Eodicyno* AZ, *Eodicynodon* Assemblage Zone; Ind, Induan; Olen, Olenekian; *Pristerog* AZ, *Pristerognathus* Assemblage Zone; Roa, Roadian; *Tapinoceph* AZ, *Tapinocephalus* Assemblage Zone; *Tropido* AZ, *Tropidostoma* Assemblage Zone; Wor, Wordian.

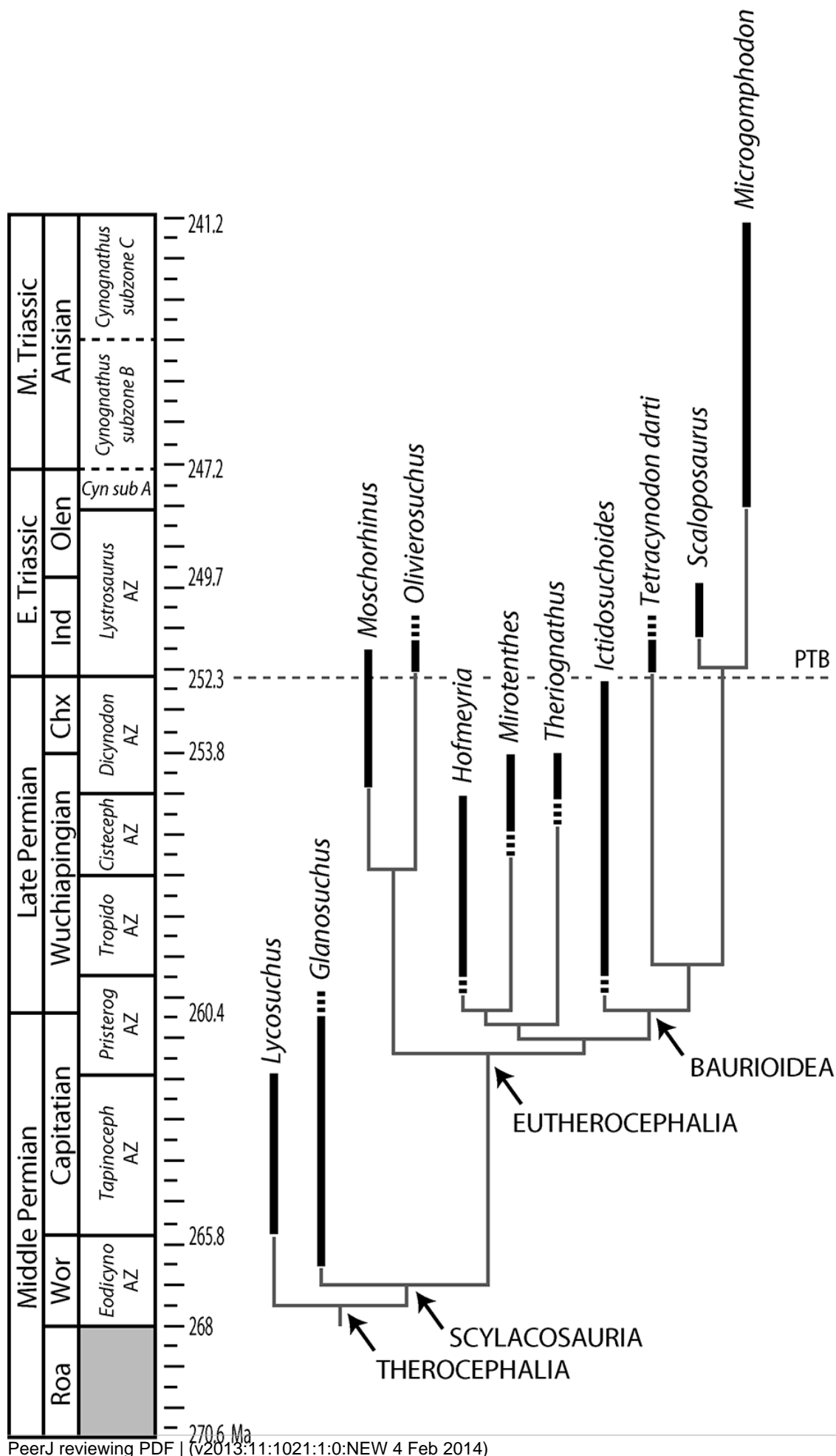


# Figure 2

Bone microstructure in selected basal therocephalians and Permo-Triassic eutheriocephalians.

**A**, Middle Permian *Lycosuchus* (SAM-PK-K9012), femur midshaft, dorsal cortex showing subplexiform fibrolamellar bone viewed under non-polarized light. **B**, Middle Permian *Lycosuchus* (SAM-PK-9084), ulna midshaft, cortical fibrolamellar bone viewed at high magnification showing reticular canals in a woven-fibered matrix (crossed-nicols with wave plate). **C**, Scylacosauridae indet. (CGS R300), humerus midshaft, cortex viewed at low magnification showing growth marks (crossed-nicols with wave plate). **D**, Early Triassic akidnognathid *Olivierosuchus* (NMQR 3605), humerus midshaft, cortical fibrolamellar bone showing thick zone of reticular fibrolamellar bone followed by parallel-fibered bone and a LAG (crossed-nicols with wave plate). **E**, *Olivierosuchus* (SAM-PK-K10617), femur midshaft, close-up of primary osteons and woven-fibered interstitial matrix (crossed-nicols with wave plate). **F**, Late Permian hofmeyriid *Mirotenthes* (SAM-PK-K6511), femur midshaft, cortical parallel-fibered bone showing annular growth marks (crossed-nicols with wave plate). **G**, Late Permian whaitsiid *Theriognathus* (NMQR 3375), femur midshaft, cortical fibrolamellar bone viewed at medium magnification showing growth marks (non-polarized light). Arrows denote growth marks. Detailed descriptions and photomicrographs are provided in the Supporting Data file. Abbreviations: pfb, parallel-fibered bone; po, primary osteon; re, reticular fibrolamellar bone.



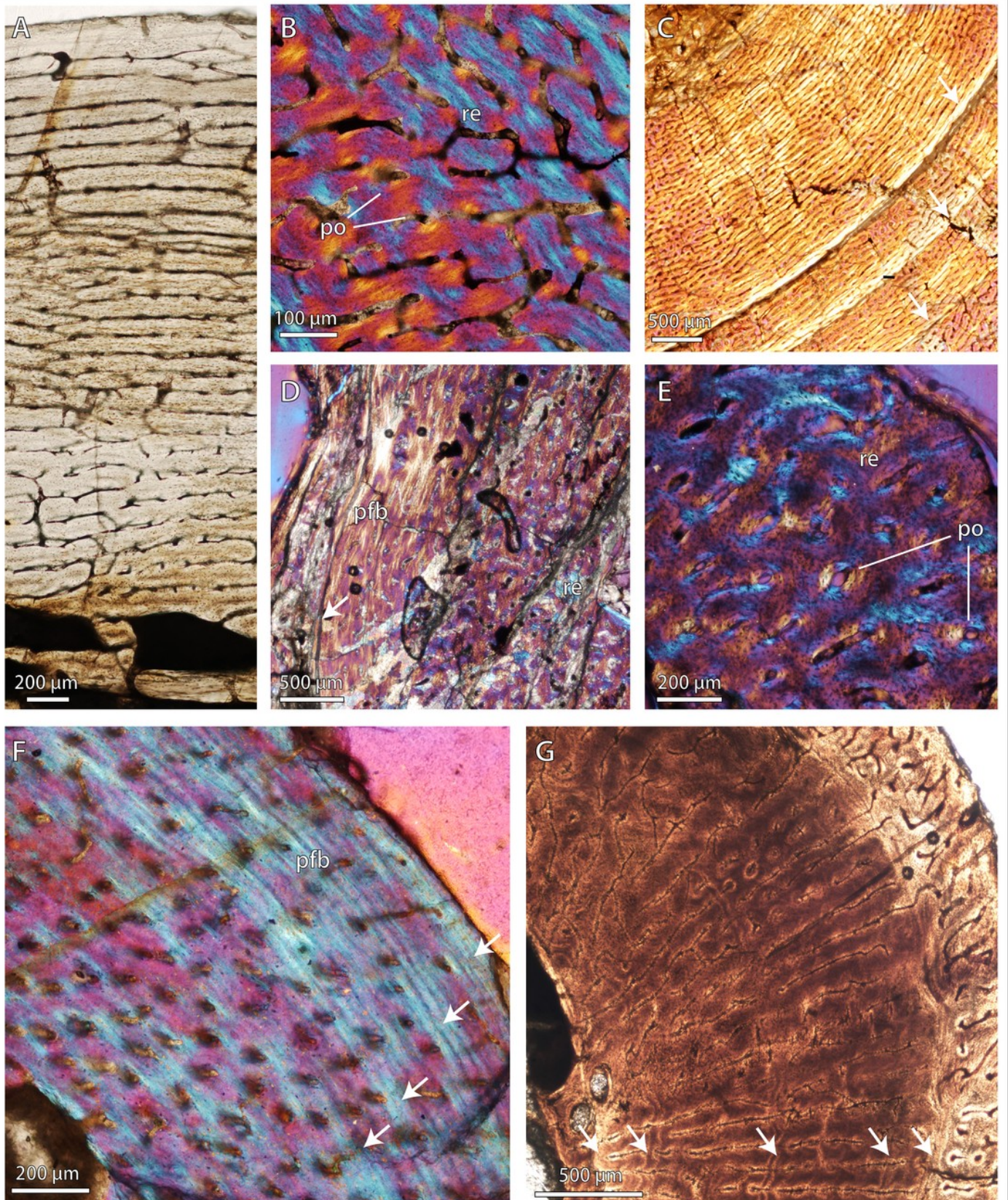




# Figure 3

Bone microstructure in selected Permo-Triassic baurioid eutheriocephalians.

**A**, Late Permian *Ictidosuchoides* subadult (SAM-PK-8659), radius midshaft, cortex and inner cancellous bony scaffold (crossed-nicols with wave plate). **B**, *Ictidosuchoides* adult (BP/1/4092), humerus midshaft, cortex with longitudinal and reticular primary osteons and growth marks (crossed-nicols with wave plate). **C**, Early Triassic *Tetracynodon* (NMQR 3745), humerus midshaft, cortex showing inner fibrolamellar bone and sparsely vascularized outer parallel-fibered bone (crossed-nicols with wave plate). **D**, Early Triassic *Scaloposaurus* (SAM-PK-K4638), humerus midshaft, cortex showing longitudinal and reticular fibrolamellar bone deposition followed by a thin collar of lamellar bone in the subperiosteal region (crossed-nicols with wave plate). **E**, Middle Triassic bauriid *Microgomphodon* (NMQR 3605), humerus midshaft, cortex showing reticular fibrolamellar bone with no growth marks (crossed-nicols with wave plate). **F**, *Microgomphodon* (NMQR 3605), femur midshaft, cortex showing reticular fibrolamellar bone (crossed-nicols with wave plate). Arrows denote growth marks. Detailed descriptions and photomicrographs are provided in the Supporting Data file. Abbreviations: pfb, parallel-fibered bone; re, reticular fibrolamellar bone.

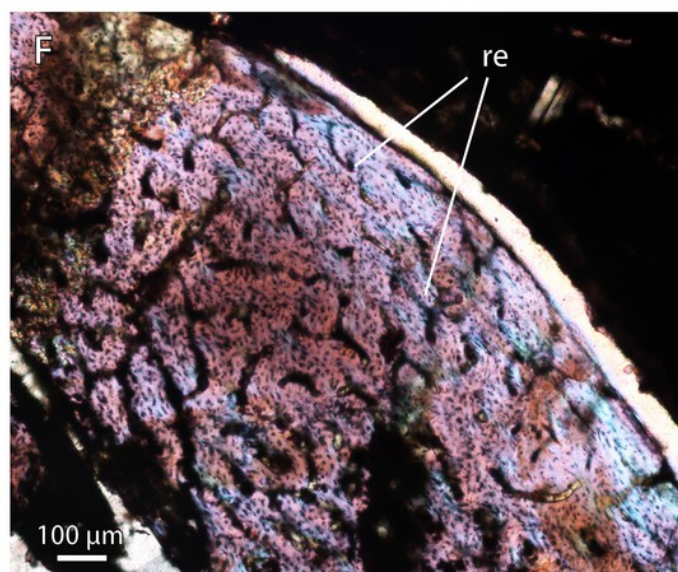
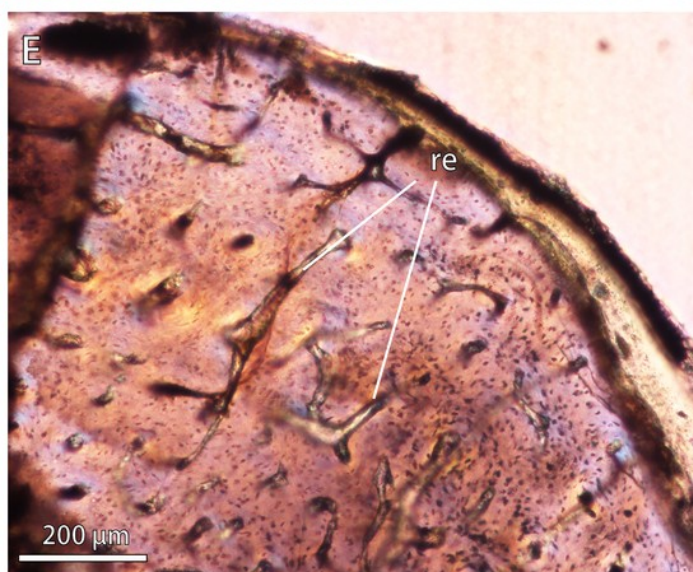
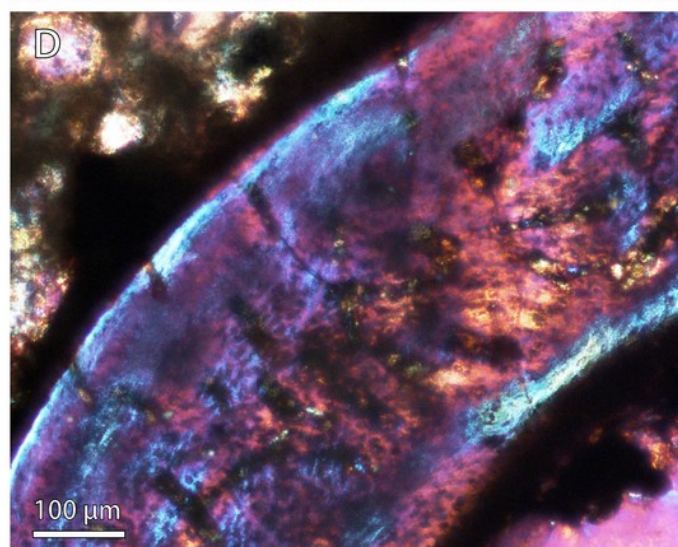
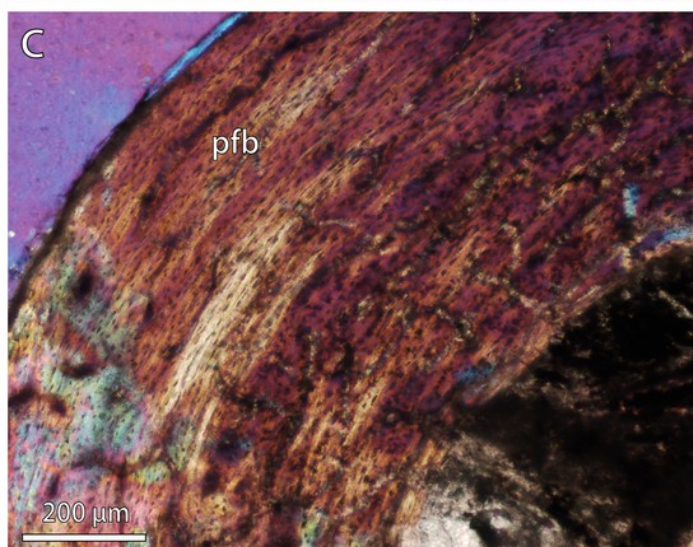
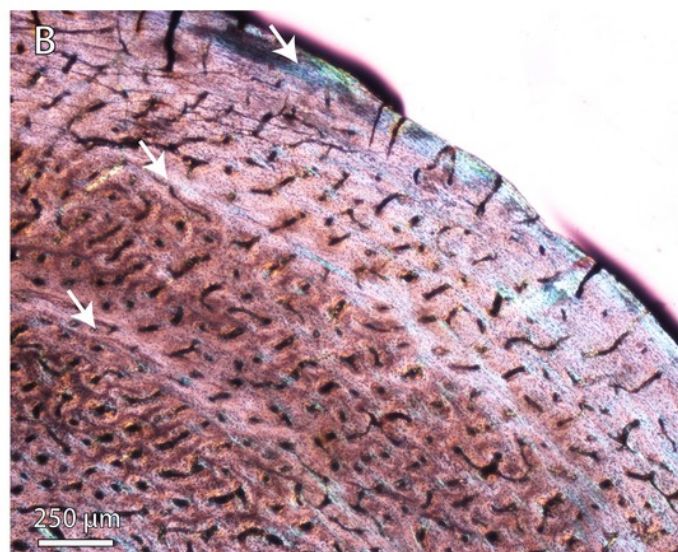
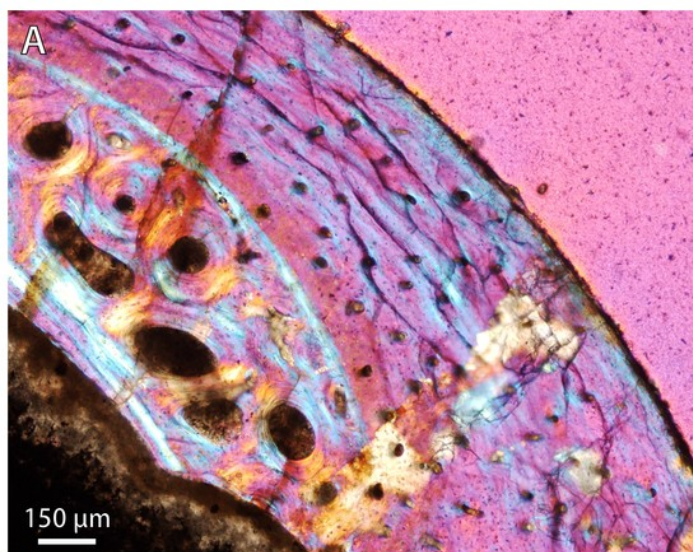




# Figure 4

Linear regression of vascular growth proxies against size (midshaft cross-sectional area) from limb bone elements.

**A**, Mean cortical vascularity (%CV) against midshaft cross-sectional area. **B**, Mean primary osteon diameter (*POD*) against midshaft cross-sectional area. **C**, mean %CV against mean *POD*. All correlations between vascular growth proxies and size are strongly positively correlated for both propodials (solid regression line) and epipodials (dashed regression line) (see statistical results in Table 2). Blue circles = propodials. Red circles = epipodials.

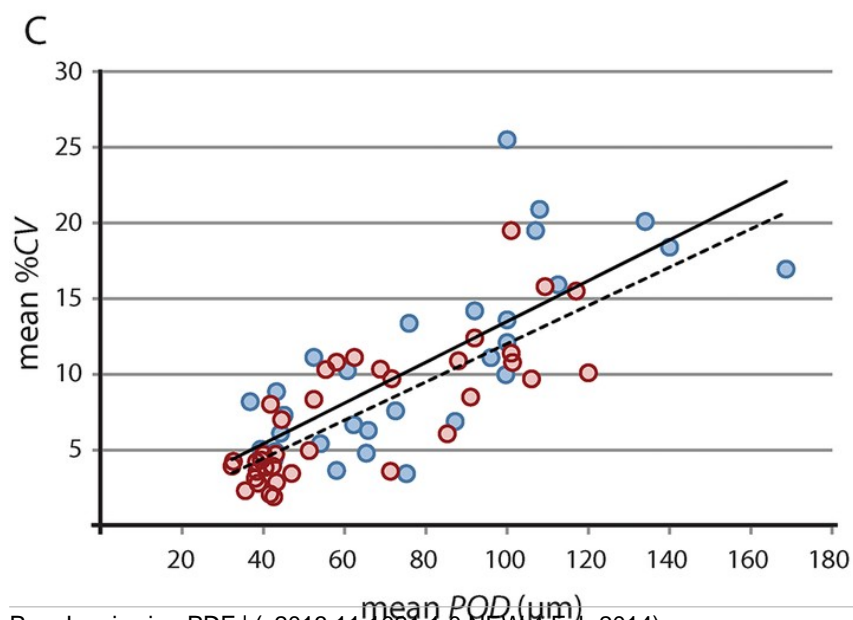
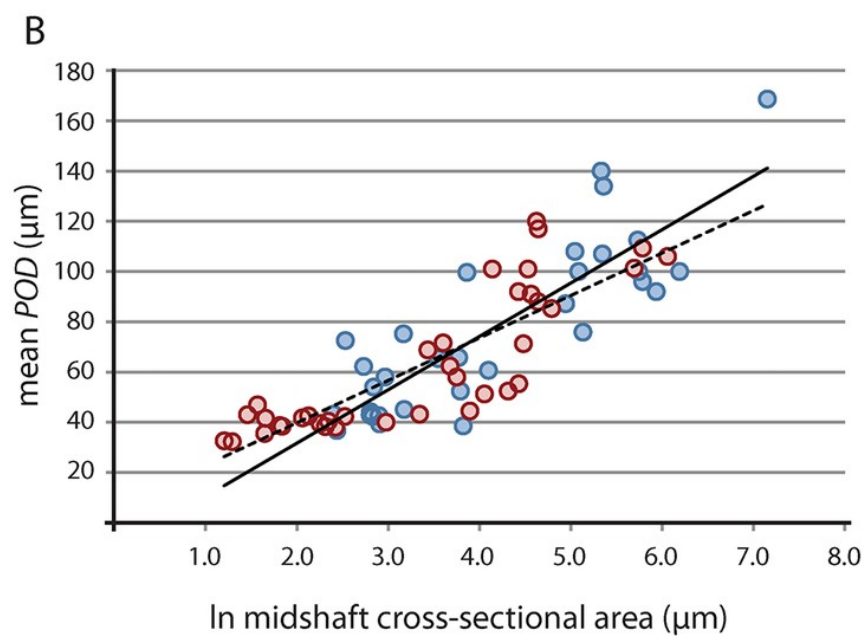
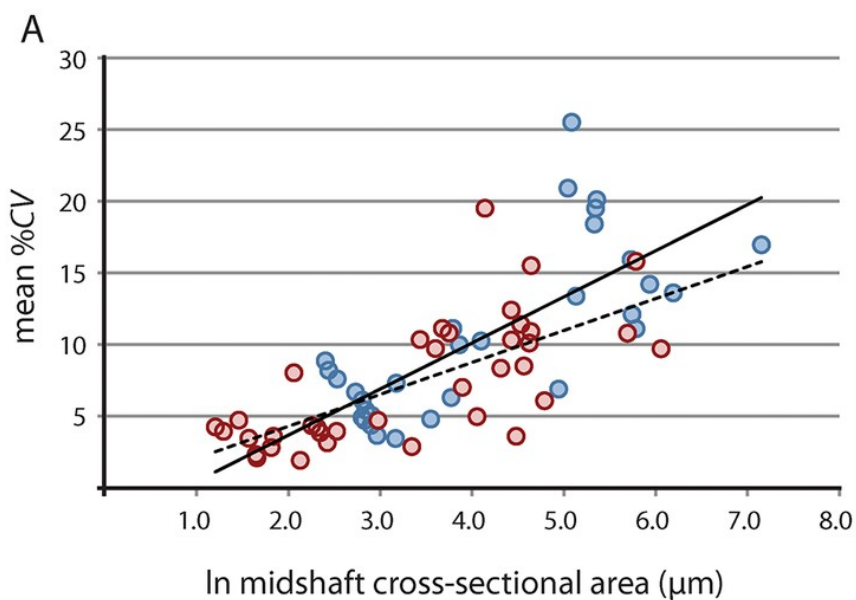


# Figure 5

Comparison of bone histology and microvasculature in Permian *Therapsid* and *Moschorhinus*.

**A**, *Therapsid* (NMQR 3375) femur midshaft cortex (non-polarized light). **B**, *Moschorhinus* (NMQR 3939) humerus midshaft cortex (non-polarized light). Note the greater overall degree of vascularity in 'B.'

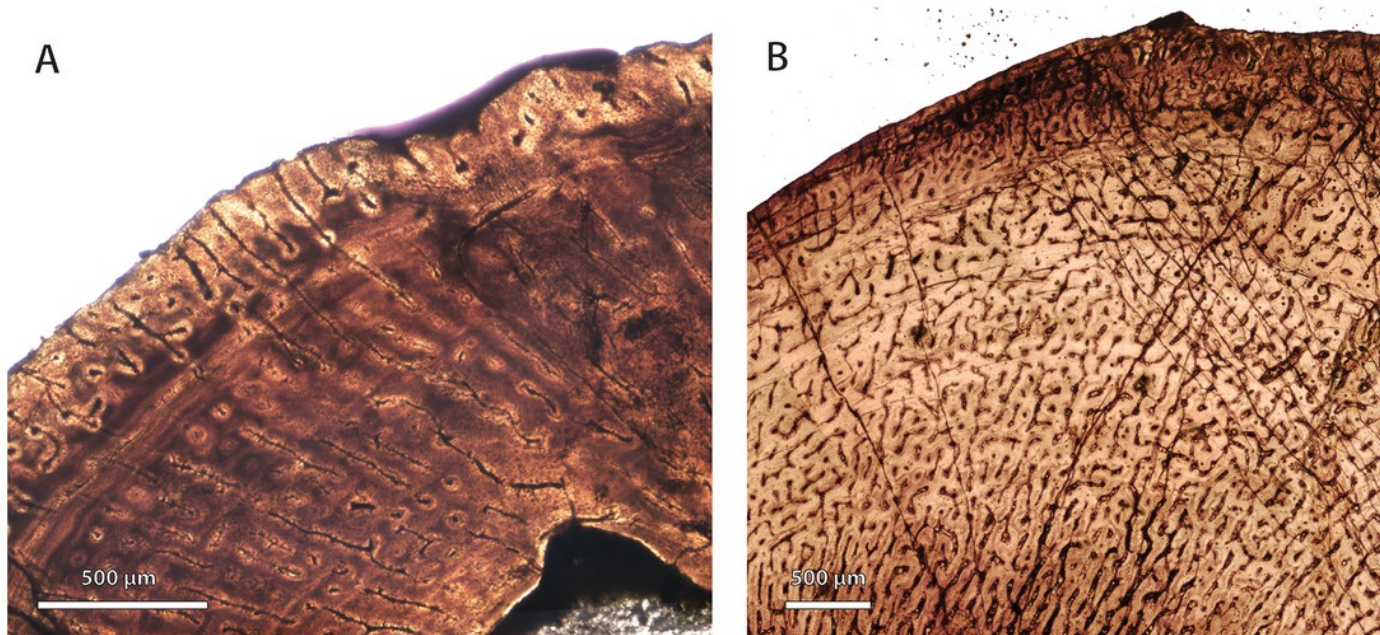


# Figure 6

Mirror phylogenies of Permo-Triassic therocephalians sampled for bone histology (scaled to geologic time).

Phylogenetic character mapping of histological traits estimated from propodials (left) and epidpodials (right) reveals comparable ancestor-descendant changes for each pool of skeletal elements. **A**, average cortical vascularity (%CV). **B**, average primary osteon diameter (*POD*). **C**, relative bone wall thickness (*RBT*). Ancestral states were reconstructed using squared-change parsimony in Mesquite version 2.0 (Maddison and Maddison, 2007).

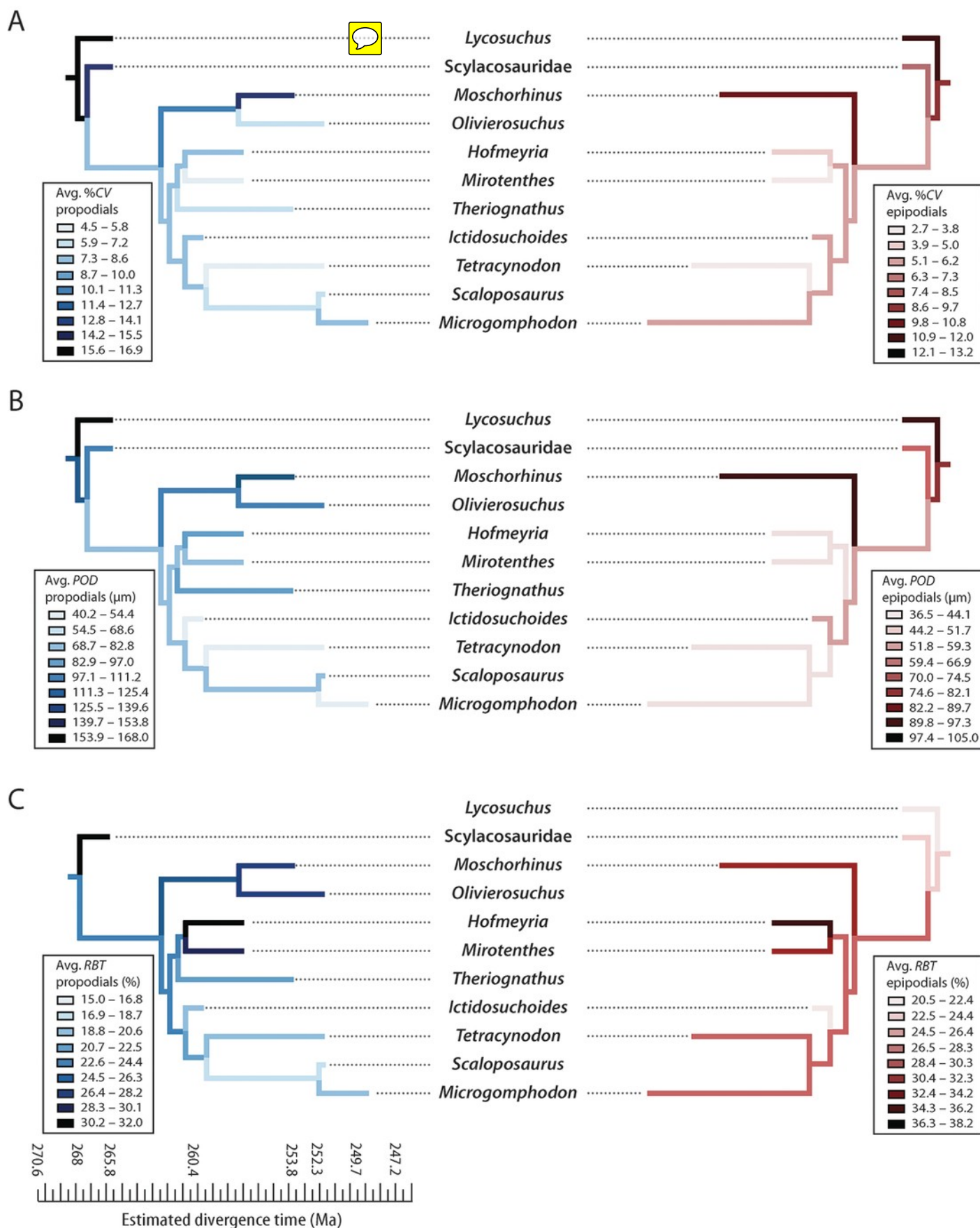


# Figure 7

Summary of evolution of size and bone microstructural traits.

Black bars represent stratigraphic ranges of taxa that were sampled histologically. Numbers in parentheses to right of black bars denote maximum size of taxon in interval of first appearance. Tree topology and ranges from Huttenlocker, 2013 and in press. In graph at top of figure, circles represent average %CV and squares average POD of propodials (blue) and epipodials (red). Abbreviations: Chx, Changxingian; *Cisteceph* AZ, *Cistecephalus* Assemblage Zone; *Cyn* sub A, *Cynognathus* subzone A; *Eodicyno* AZ, *Eodicynodon* Assemblage Zone; Ind, Induan; Olen, Olenekian; *Pristerog* AZ, *Pristerognathus* Assemblage Zone; Roa, Roadian; *Tapinoceph* AZ, *Tapinocephalus* Assemblage Zone; *Tropido* AZ, *Tropidostoma* Assemblage Zone; Wor, Wordian. 